Relating gravitational wave constraints from primordial nucleosynthesis, pulsar timing, laser interferometers, and the CMB: Implications for the early universe

Latham A. Boyle[1,2] and Alessandra Buonanno[3]

[1]*Canadian Institute for Theoretical Astrophysics (CITA), University of Toronto, 60 St. George Street, Toronto, Ontario, M5S 3H8, Canada*

[2]*Department of Physics, Princeton University, Princeton, New Jersey 08544, USA*

[3]*Maryland Center for Fundamental Physics, Department of Physics, University of Maryland, College Park, Maryland 20742, USA*

(Received 23 December 2007; published 18 August 2008)

We derive a general equation relating the gravitational-wave observables r and $\Omega_0^{\rm gw}(f)$; or the observables $\Omega_0^{\rm gw}(f_1)$ and $\Omega_0^{\rm gw}(f_2)$. Here, r is the so-called ''tensor-to-scalar ratio,'' which is constrained by cosmic-microwave-background experiments; and $\Omega_0^{\rm gw}(f)$ is the energy spectrum of primordial gravitational waves, which is constrained, e.g., by pulsar-timing measurements, laser-interferometer experiments, and the standard big bang nucleosynthesis bound. Differentiating this equation yields a new expression for the tilt $d\ln\Omega_0^{\rm gw}(f)/d\ln f$ of the present-day gravitational-wave spectrum. The relationship between r and $\Omega_0^{\rm gw}(f)$ depends sensitively on the uncertain physics of the early universe, and we show that this uncertainty may be encapsulated (in a model-independent way) by two quantities: $\hat{w}(f)$ and $\hat{n}_t(f)$, where $\hat{n}_t(f)$ is a certain logarithmic average over $n_t(k)$ (the primordial tensor spectral index); and $\hat{w}(f)$ is a certain logarithmic average over $\tilde{w}(a)$ (the effective equation-of-state parameter in the early universe, after horizon re-entry). Here, the *effective* equation-of-state parameter $\tilde{w}(a)$ is a combination of the *ordinary* equation-of-state parameter $w(a)$ and the bulk viscosity $\zeta(a)$. Thus, by comparing observational constraints on r and $\Omega_0^{\rm gw}(f)$, one obtains (remarkably tight) constraints in the $\{\hat{w}(f), \hat{n}_t(f)\}$ plane. In particular, this is the best way to constrain (or detect) the presence of a stiff energy component (with $w > 1/3$) in the early universe, prior to big bang nucleosynthesis. (The discovery of such a component would be no more surprising than the discovery of a tiny cosmological constant at late times!) Finally, although most of our analysis does *not* assume inflation, we point out that if cosmic-microwave-background experiments detect a nonzero value for r, then we will immediately obtain (as a free by-product) a new upper bound $\hat{w} \lesssim 0.55$ on the logarithmically averaged effective equation-of-state parameter during the ''primordial dark age'' between the end of inflation and the start of big bang nucleosynthesis.

DOI: 10.1103/PhysRevD.78.043531 PACS numbers: 98.80.Es, 04.80.Nn, 98.80.Cq, 98.80.Jk

I. INTRODUCTION

A variety of different experiments (some already operating, others in various stages of development) are hoping to detect gravitational waves (tensor perturbations) from the early universe. In particular, at long wavelengths, cosmic-microwave-background (CMB) experiments [1–13] will measure (or tightly constrain) the so-called tensor-to-scalar ratio r by searching for its characteristic ''B mode'' imprint in the CMB polarization anisotropy [14–16]. And on shorter wavelengths, various techniques—including pulsar-timing (PT) [17–19] and laser-interferometer (LI) experiments [20–26]—will measure or constrain the present-day gravitational-wave energy spectrum $\Omega_0^{\rm gw}(f)$.

The coming decade is likely to see exciting progress in this area. At the lowest frequencies, CMB polarization experiments will either detect gravitational waves from inflation [27–36], or else rule out the simplest (and arguably the most compelling) inflationary models [36]. At intermediate frequencies, pulsar timing *arrays* [18,19] will reach far beyond the gravitational-wave sensitivity of individual pulsars. And at high frequencies, the sensitivity of ground-based gravitational-wave detectors (and also the space-based mission LISA, if it is launched) will surpass the so-called ''standard big bang nucleosynthesis (sBBN) bound'' by several orders of magnitude, and thus place genuinely new constraints on the primordial gravitational-wave signal at high frequencies.

Since primordial gravitational waves provide a rare and precious window onto the extremely high-energy physics of the infant universe, it is essential to think carefully about the information that they carry.

In this paper we derive Eq. (1) relating the long-wavelength observable r to the short-wavelength observable $\Omega_0^{\rm gw}(f)$, under rather minimal and general assumptions about the highly uncertain physics of the early universe. The key point about this equation is that all of the early-universe uncertainty is neatly and precisely absorbed into four parameters $\{\hat{w}, \hat{n}_t, C_2, C_3\}$, each of which has a distinct physical meaning and is defined below. Furthermore, the relationship between r and $\Omega_0^{\rm gw}$ is much more sensitive to $\hat{w}$ and $\hat{n}_t$ than to C_2 and C_3, so that observational constraints on r and $\Omega_0^{\rm gw}$ are most naturally

and model-independently interpreted as constraints on the early-universe quantities $\hat{w}$ and $\hat{n}_t$. We proceed to derive the constraints on $\hat{w}$ and $\hat{n}_t$ that follow from various possible combinations of present and future gravitational wave constraints. For example: if CMB experiments succeed in detecting a nonzero value for r, then (by combining with sBBN) we can immediately infer a nontrivial constraint in the $\{\hat{w}, \hat{n}_t\}$ plane, as shown in Fig. 5. By constraining $\hat{w}$ in this way, gravitational waves may provide the best means of constraining (or detecting) a primordial energy component with an unexpectedly "stiff" equation of state $w > 1/3$.

The two quantities $\hat{w}$ and $\hat{n}_t$ are defined by Eqs. (7)–(9), and explained in detail in Sec. III. For now, let us briefly discuss their physical meaning: $\hat{n}_t(f)$ is the logarithmic average (over a certain range of comoving wave number k) of the primordial tensor spectral index $n_t(k)$; and $\hat{w}(f)$ is the logarithmic average (over a certain range of the cosmological scale factor a) of the effective equation-of-state parameter $\tilde{w}(a)$ in the early universe (*after* horizon reentry). Here, the *effective* equation-of-state parameter $\tilde{w}(a)$ is a combination of the *ordinary* equation-of-state parameter $w(a)$ and the bulk viscosity $\zeta(a)$: see Eq. (8).

A key advantage of our current formulation in general (and of the variables $\hat{w}(f)$ and $\hat{n}_t(f)$, in particular) is that $w(a)$, $\zeta(a)$, and $n_t(k)$ may be arbitrary functions of a and k, respectively. So, in particular, we will *not* take w or n_t to be constant (or piecewise constant), as is often assumed in analytical treatments of primordial gravitational waves. When deriving Eq. (1), the quantities $\hat{w}(f)$ and $\hat{n}_t(f)$ naturally arise as the most direct and general encapsulation of the uncertain early-universe physics that enters into the relationship between r and $\Omega_0^{\rm gw}(f)$.

As an application, we will stress that comparison of r and $\Omega_0^{\rm gw}(f)$ provides the most powerful way to constrain the equation-of-state parameter $w(a)$ during the "primordial dark age." Here, we use the phrase primordial dark age to refer to the epoch separating the end of inflation from the start of big bang nucleosynthesis (BBN). Note that, on a logarithmic scale, this primordial dark age spans a large fraction of cosmic history: the energy scale of BBN is $\sim 10^{-3}$ GeV, while the energy scale at the end of inflation may exceed 10^{16} GeV. And yet, although there is a standard *theoretical* picture of how the Universe behaves during this early epoch, we currently have essentially no direct *observational* constraints.

In fact, there are several reasons to be nervous about one of the key (implicit) assumptions in the standard picture of the primordial dark age: namely, the assumption that the equation-of-state satisfies $w \leq 1/3$. The first reason to worry is rather general: since the energy density of a cosmological matter component scales as $\rho \propto a^{-3(1+w)}$, components with lower w dilute more slowly. Thus, just as an exotic component with w sufficiently *low* will tend to dominate the cosmic energy budget at sufficiently *late* times (think of "dark energy" with $w < -1/3$), an exotic component with w sufficiently *high* (call it "stiff energy" with $w > +1/3$) will tend to dominate the cosmic energy budget at sufficiently *early* times (see Fig. 1). Indeed, as we look backward past BBN, the primordial dark age provides a huge window in which a stiff energy component might overtake radiation as the dominant component in the cosmic energy budget, without coming into conflict with any current observational constraints. It is also worth noting that there are perfectly sensible energy components with $w > 1/3$, which might be present in the early universe. For example, a homogeneous scalar field $\phi(t)$ with vanishing (or negligible) potential energy $V(\phi) = 0$ has $w = 1$; and, in fact, supergravity and string theory seem to naturally predict many (embarrassingly many!) scalar moduli fields with precisely this property. Furthermore, various authors [37–47] have considered inflation models in which the inflaton field itself experiences a period of free ($w = 1$) evolution at the end of inflation; or some other equation of state stiffer than radiation [48–53].

"Stiff ($w > 1/3$) energy" in the early universe may seem like an exotic possibility. But would the discovery of "stiff energy" at early times be any more surprising than our apparent discovery of "dark energy" at late times? One lesson that we have learned from dark matter and dark energy is that the Universe has an unmistakable penchant for new and unexpected energy components; and it is important to check for these components observationally,

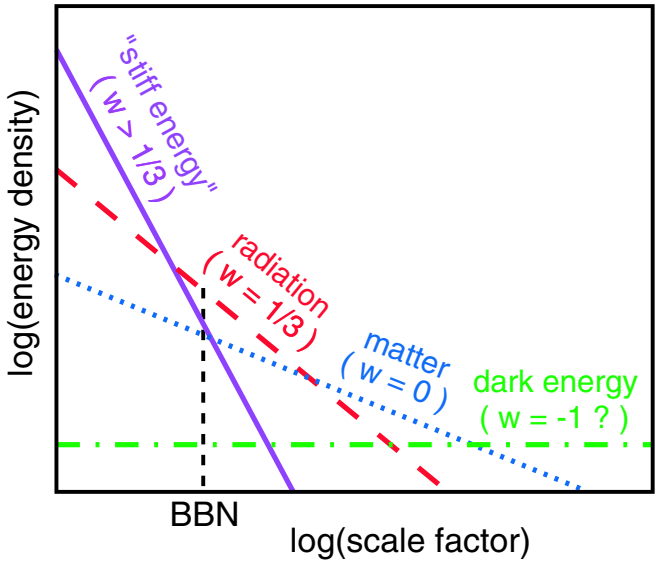

FIG. 1 (color online). How the components of the cosmological energy budget scale with cosmological expansion: "stiff energy" (solid purple line), radiation (long-dashed red line), matter (dotted blue line), and dark energy (dotted-dashed green line). Components with higher w tend to dominate at earlier times. Our universe may be dominated by a "stiff energy" component (with $w > 1/3$) prior to big bang nucleosynthesis (but after inflation).

if possible, rather than simply assuming that they are not there. We will stress that the comparison of constraints on r and $\Omega_0^{\rm gw}(f)$ provides the best means for carrying out such a check.[1]

One of the most important results in this paper comes from considering the relationship between the CMB constraint on r and the sBBN constraint on $\Omega_0^{\rm gw}(f)$. If CMB polarization experiments succeed in detecting a nonzero value for the primordial tensor-to-scalar ratio r, this will be widely interpreted as providing evidence for inflation. But we show that, if these primordial tensor fluctuations are really generated by inflation, then (in combination with the current sBBN constraint on $\Omega_0^{\rm gw}(f)$), this will also imply an immediate and important supplementary result: namely, a remarkably tight bound in the $\{\hat{w}(f), \hat{n}_t(f)\}$ plane. This bound in the $\{\hat{w}(f), \hat{n}_t(f)\}$ plane is derived in Sec. VII, and shown in Fig. 5.

If CMB polarization experiments detect a nonzero value for r, then the bound depicted in Fig. 5 will be a qualitatively new piece of model-independent information about the early universe—which is very exciting, since such information is notoriously hard to obtain! One way to look at the bound is as follows: If we assume that the bulk viscosity $\zeta(a)$ is negligible after inflation, and also that the primordial tensor power spectrum $\Delta_h^2(k)$ is nearly flat (which is a prediction of inflation), then we obtain an upper bound $\langle w \rangle < 0.55$ on the logarithmic average of the equation-of-state parameter $w(a)$ during the primordial dark age separating the end of inflation from the BBN epoch.

It is important to clarify the range of validity of our analysis. When we use $\Omega_0^{\rm gw}(f)$ in this paper, we are referring only to *primordial* gravitational waves—and, more specifically, only to those gravitational waves that were generated well *before* the corresponding comoving wavelength "entered the Hubble horizon" (i.e., became shorter than the instantaneous Hubble length). Apart from this restriction, the results are quite general, and make no assumptions about the physical mechanism responsible for generating the gravitational waves. For example, our analysis applies to the primordial gravitational-wave spectrum generated during inflation; and it applies equally well to the primordial gravitational-wave spectra generated by the "pre-big bang" [56,57] and "cyclic/ekpyrotic" [58–60] alternatives to inflationary cosmology; and, although all of the previous three examples (inflationary, pre-big bang, and ekpyrotic/cyclic cosmology) generate primordial gravitational waves through the cosmological amplification of quantum fluctuations, our analysis would also apply to models that generate primordial gravitational waves via some completely different mechanism (as long as they are generated *prior* to horizon entry).[2] On the other hand, our analysis *does not* apply, e.g., to the gravitational-wave spectrum produced by the incoherent superposition of signals from merging binary stars [61], or by a hypothetical period of preheating after inflation [62], or by bubble collisions after a cosmological phase transition [63]—since all of these production mechanisms result in gravitational waves that are *shorter* than the instantaneous Hubble length at the time when they are generated.

This paper is organized as follows. Sec. II introduces some notation. In Sec. III, we present and explain Eq. (1), which relates r and $\Omega_0^{\rm gw}(f)$, and will serve as the basis for most of our analysis. In Sec. IV, we use Eq. (1) to derive two simple results. The first result is Eq. (15), which expresses the relationship between $\Omega_0^{\rm gw}(f_1)$ and $\Omega_0^{\rm gw}(f_2)$—that is, two different short-wavelength constraints (e.g., from LIGO and LISA) at two different frequencies f_1 and f_2. The second result is Eq. (19), which significantly generalizes previous expressions for the tilt $d\ln\Omega_0^{\rm gw}(f)/d\ln k$ of the present-day energy spectrum of primordial gravitational waves. In Sec. V, we analyze the implications of combining CMB constraints on r with LI and PT constraints on $\Omega_0^{\rm gw}(f)$. The section breaks into four parts, depending on whether we suppose that CMB and LI/PT experiments have detected the gravitational-wave background, or merely bounded it from above. The results are summarized in Figs. 2–4. In Sec. VI, we discuss the following point: If LI or PT experiments detect an unexpectedly strong stochastic gravitational-wave signal $\Omega_0^{\rm gw}(f)$, then there is a rough observational consistency check that this signal should satisfy, if it is truly of primordial origin. In Sec. VII, we analyze the constraint in the $\{\hat{w}(f), \hat{n}_t(f)\}$ plane that follows from combining a CMB *detection* of r with the sBBN bound on $\Omega_0^{\rm gw}(f)$. As mentioned above, this constraint is rather strong; and it is also quite insensitive to the detected value of r: see Fig. 5. Finally, we conclude in Sec. VIII. Some of the key equations in the text are derived in appendices: in particular, Eq. (1) is derived in Appendix A, and Eqs. (12) and (13) are derived in Appendix B. Appendix C lists a few numbers that are useful for converting our various algebraic expressions into numerical results and plots.

II. NOTATION

Throughout this paper, we will often use subscripts to indicate the time at which a quantity is to be evaluated. For example, a quantity with subscript "0" is evaluated at the

[1] It is also worth mentioning that an exotic equation-of-state parameter $w \neq 1/3$ in the early universe will effect the relic abundance of particles that freeze out at sufficiently early times [54,55].

[2] A caveat is that the derivation of Eq. (13) specifically applies to standard inflation [28] (and *not* to pre-big bang [56] or ekpyrotic/cyclic [58,59] models). But this is a very mild caveat, since Eq. (13) is used only in Sec. VII, which deals with models that produce a *detectable* value for r (which pre-big bang and ekpyrotic/cyclic models do not [57,58,60]).

present time, a quantity with subscript "c" is evaluated at the redshift z_c (defined in Sec. III), and a quantity with subscript "k" is evaluated when the comoving wave number k "re-enters the Hubble horizon" (i.e., crosses from $k < aH$ to $k > aH$).

We will also use units in which the speed of light is unity, $c = 1$.

III. THE STARTING POINT: A REFINED RELATIONSHIP BETWEEN r AND $\Omega_0^{\rm gw}(f)$

Primordial gravitational-wave measurements probe two basic quantities. On long wavelengths, CMB polarization experiments constrain the tensor-to-scalar ratio r. And on shorter wavelengths, various techniques constrain the present-day gravitational-wave energy spectrum $\Omega_0^{\rm gw}(f)$. In Appendix A, we derive the equation relating r and $\Omega_0^{\rm gw}(f)$. The result is

$$\Omega_0^{\rm gw}(f) = [A_1 A_2^{\hat{\alpha}(f)} A_3^{\hat{n}_t(f)}] r. \tag{1}$$

As we shall see in a moment, the factor A_1 is roughly independent of the gravitational-wave frequency f, while the two factors A_2 and A_3 are both proportional to f, so that $\Omega_0^{\rm gw}(f)$ is roughly proportional to $f^{\hat{\alpha}(f)+\hat{n}_t(f)}$.

Now let us carefully explain the meaning of each quantity appearing in Eq. (1)—namely, the gravitational-wave observables $\{\Omega_0^{\rm gw}(f), r\}$, the factors $\{A_1, A_2, A_3\}$, and the exponents $\{\hat{\alpha}(f), \hat{n}_t(f)\}$.

The present-day gravitational-wave energy spectrum

$$\Omega_0^{\rm gw}(f) \equiv \frac{1}{\rho_0^{\rm crit}} \frac{d\rho_0^{\rm gw}}{d\ln f} \tag{2}$$

represents the present-day gravitational-wave energy density ($\rho_0^{\rm gw}$) per logarithmic frequency interval, in units of the present-day "critical density" $\rho_0^{\rm crit} \equiv 3H_0^2/(8\pi G_N)$, where H_0 is the present-day value of the Hubble expansion rate, and G_N is Newton's gravitational constant.

The tensor-to-scalar ratio

$$r \equiv \frac{\Delta_h^2(k_{\rm cmb})}{\Delta_{\mathcal{R}}^2(k_{\rm cmb})} \tag{3}$$

is the ratio of the primordial tensor power spectrum $\Delta_h^2(k_{\rm cmb})$ (defined in Appendix A) to the primordial scalar power spectrum $\Delta_{\mathcal{R}}^2(k_{\rm cmb})$ at the CMB wave number $k_{\rm cmb}$.[3] Our definition of the tensor-to-scalar ratio matches the convention used, e.g., by the WMAP experiment [64,65] and the CAMB numerical code [66]; but beware that there are several alternative definitions/conventions floating around in the literature. The CMB wave number $k_{\rm cmb}$ is the comoving wave number at which CMB experiments report their constraints on $\Delta_{\mathcal{R}}^2$, Δ_h^2, and r: e.g., the WMAP experiment [64,65] uses $k_{\rm cmb}/a_0 = 0.002\ {\rm Mpc}^{-1}$, where a_0 is the present-day value of the cosmological scale factor.

Next, consider the 3 factors $\{A_1, A_2, A_3\}$ appearing in Eq. (1). They are given by

$$A_1 \equiv \frac{C_2(k) C_3(k) \Delta_{\mathcal{R}}^2(k_{\rm cmb}) \gamma}{24}, \tag{4a}$$

$$A_2 \equiv \left(\frac{2\pi f}{H_0}\right) \frac{1}{(1+z_c)\gamma^{1/2}}, \tag{4b}$$

$$A_3 \equiv \left(\frac{2\pi f}{H_0}\right) \frac{H_0}{(k_{\rm cmb}/a_0)}, \tag{4c}$$

where

$$\gamma \equiv \frac{g_*(z_c)}{g_*(0)} \frac{g_{*s}^{4/3}(0)}{g_{*s}^{4/3}(z_c)} \Omega_0^{\rm rad}. \tag{5}$$

In these expressions, the comoving wave number k is related to the physical frequency f through the relation $k/a_0 = 2\pi f$. The cosmological scale factor a is related to the cosmological redshift z through the relation $a_0/a = 1 + z$. In particular, z_c denotes the highest redshift at which we *know* that the Universe was radiation dominated (i.e., the redshift at the end of the "primordial dark age" discussed in the Introduction). Given our present observational knowledge of the early universe, it is natural to choose z_c to be the redshift of BBN $z_{\rm bbn}$; but in the future, as our knowledge of the early universe improves, a different choice (i.e., a higher redshift z_c) may become more appropriate. The factors $g_*(z)$ and $g_{*s}(z)$, which measure the effective number of relativistic degrees of freedom in the Universe at redshift z, are conveniently *defined* as follows: If $\rho(z)$, $s(z)$, and $T(z)$ denote, respectively, the energy density, entropy density, and temperature at redshift z, then $\rho(z) = (\pi^2/30) g_*(z) T^4(z)$ and $s(z) = (2\pi^2/45) g_{*s}(z) T^3(z)$. Note that for $g_*(0)$, $g_{*s}(0)$, and $\Omega_0^{\rm rad}$, one should use the values that these parameters would have *if all three neutrino species were massless*. (For explicit numerical values, see Appendix C.) These are the correct values to use in Eq. (5) even though, in reality, neutrinos have mass. For a detailed discussion of the "correction factors" $C_2(k)$ and $C_3(k)$, including definitions and explicit expressions, see Appendix A and Ref. [67]. For now, it is enough to note that $C_2(k)$ and $C_3(k)$ are both $\mathcal{O}(1)$, which means that they will not play a very significant role in this paper (although in other contexts they can be interesting and important, see Ref. [67]).

Finally, consider the two exponents, $\hat{\alpha}(f)$ and $\hat{n}_t(f)$, that appear in Eq. (1). The first exponent $\hat{\alpha}(f)$ is given by

$$\hat{\alpha}(f) \equiv 2\left(\frac{3\hat{w}(f) - 1}{3\hat{w}(f) + 1}\right), \tag{6}$$

where $\hat{w}(f)$ is the logarithmic average

$$\hat{w}(f) \equiv \frac{1}{\ln(a_c/a_k)} \int_{a_k}^{a_c} \tilde{w}(a) \frac{da}{a} \tag{7}$$

[3] Note that, in Eqs. (1) and (4a), we could trade the more commonly used observables r and $\Delta_{\mathcal{R}}^2(k_{\rm cmb})$ for the single (but less commonly used) observable $\Delta_h^2(k_{\rm cmb})$.

of the *effective* equation-of-state parameter $\tilde{w}(a)$ from a_k (the scale factor when $k = 2\pi a_0 f$ re-entered the horizon) to a_c (the scale factor at redshift z_c). Here, the effective equation-of-state parameter $\tilde{w}(a)$ is given by

$$\tilde{w}(a) \equiv w(a) - \frac{8\pi G_N \zeta(a)}{H(a)}, \tag{8}$$

where $w(a) = p(a)/\rho(a)$ is the *ordinary* equation-of-state parameter [i.e., the ratio of the total cosmological pressure $p(a)$ to the total cosmological energy density $\rho(a) = \rho^{\rm crit}(a)$], $H(a)$ is the Hubble expansion rate, and $\zeta(a)$ is the bulk viscosity of the cosmological fluid (see Secs. 2.11 and 15.11 in Ref. [68]). The second exponent $\hat{n}_t(f)$ is given by the logarithmic average

$$\hat{n}_t(f) \equiv \frac{1}{\ln(k/k_{\rm cmb})} \int_{k_{\rm cmb}}^{k} n_t(k') \frac{dk'}{k'} \tag{9}$$

of the primordial tensor tilt $n_t(k')$ over the wave number range $k_{\rm cmb} < k' < k$. Here, the primordial tensor tilt $n_t(k)$ is defined as the logarithmic slope of the primordial tensor power spectrum $\Delta_h^2(k)$ at comoving wave number k

$$n_t(k) \equiv \frac{d\ln\Delta_h^2(k)}{d\ln k}. \tag{10}$$

We again stress that the equation-of-state parameter $w(a)$ may have arbitrary a dependence, and the primordial tensor tilt $n_t(k)$ may have arbitrary k dependence. We do *not* assume that w or n_t is constant.

Let us clarify the sense in which $\Omega_0^{\rm gw}(f)$ is a "short-wavelength" gravitational-wave observable. We mean that, in Eq. (1), the quantity $\Omega_0^{\rm gw}(f)$ represents the present-day gravitational-wave energy spectrum *on scales that re-entered the Hubble horizon during the primordial dark age*: that is, after the end of inflation (or whatever process produced the primordial gravitational-wave signal), but before the redshift z_c. In other words, the frequency f that appears in Eq. (1) lies in the range

$$f_c < f < f_{\rm end}. \tag{11}$$

Here, f_c is the present-day frequency of the comoving wave number $k_c = 2\pi a_0 f_c$ that re-entered the Hubble horizon ($k_c = a_c H_c$) at redshift z_c; and $f_{\rm end}$ is the high-frequency cutoff of $\Omega_0^{\rm gw}(f)$. As shown in Appendix B, f_c is given by

$$f_c = \frac{H_0}{2\pi}(1+z_c)\gamma^{1/2} \tag{12}$$

and, if the primordial tensor spectrum is generated by inflation, then $f_{\rm end}$ is given by

$$f_{\rm end} = \frac{H_0}{2\pi}\left[\frac{\pi^2 r \Delta_{\mathcal{R}}^2(k_{\rm cmb}, \tau_i)}{16\pi G_N H_0^2} \frac{\gamma^{1-(1/2)\hat{\alpha}}}{(1+z_c)^{\hat{\alpha}}} \left(\frac{a_0 H_0}{k_{\rm cmb}}\right)^{\hat{n}_t}\right]^{1/\hat{\beta}} \tag{13}$$

where, in this equation, we have used the abbreviated notation $\{\hat{\alpha}, \hat{\beta}, \hat{n}_t\}$ for the quantities $\{\hat{\alpha}(f_{\rm end}), \hat{\beta}(f_{\rm end}), \hat{n}_t(f_{\rm end})\}$, and defined

$$\hat{\beta}(f_{\rm end}) \equiv 4 - \hat{\alpha}(f_{\rm end}) - \hat{n}_t(f_{\rm end}). \tag{14}$$

For concreteness, let us give some rough numbers: if we take $z_c = z_{\rm bbn}$ (i.e., the redshift at which the temperature was $T \approx 1$ MeV), then $f_c = f_{\rm bbn} \approx 1.8 \times 10^{-11}$ Hz; and if the primordial tensor spectrum is generated by inflation (with $\hat{n}_t \approx 0$), followed by a "standard" primordial dark age (with $\hat{w} \approx 1/3$), then $f_{\rm end} \approx 4.5 \times 10^8 r^{1/4}$ Hz.

Let us emphasize once again that the derivation of Eq. (13) is the *only* place in this paper where we assume that the primordial gravitational-wave spectrum was generated by inflation. Since most of the results in this paper do not rely on Eq. (13), their validity does *not* rely on the correctness of inflation. Indeed, we will only need Eq. (13) in Sec. VII, when we want to combine CMB and BBN constraints.

It is useful to interpret Eq. (1) as follows: From Eq. (1), we see that the relationship between r and $\Omega_0^{\rm gw}(f)$ is *much* more sensitive to the two quantities $\{\hat{w}(f), \hat{n}_t(f)\}$ than it is to the three quantities $\{A_1, A_2, A_3\}$—because $\hat{w}(f)$ and $\hat{n}_t(f)$ appear in the exponents of the huge dimensionless numbers A_2 and A_3. This means that, even though the numerical values of $\{A_1, A_2, A_3\}$ are somewhat uncertain (since, e.g., H_0 and $\Omega_0^{\rm mat}$ are measured with non-negligible error bars, and C_2 and C_3 are only known to be roughly equal to unity), these uncertainties do not significantly affect the constraints on $\hat{w}(f)$ and $\hat{n}_t(f)$ coming from Eq. (1), as we shall see in more detail below. In other words, we may think of $\{A_1, A_2, A_3\}$ as "known" quantities; so that when we measure or observationally constrain r and $\Omega_0^{\rm gw}(f)$, Eq. (1) allows us to directly infer constraints on the "unknown" quantities $\hat{w}(f)$ and $\hat{n}_t(f)$.

IV. TWO SIMPLE CONSEQUENCES

Before moving on, we note two simple results that follow directly from Eq. (1).

The first result is obtained by evaluating Eq. (1) at two different frequencies, f_1 and f_2, and taking the ratio to get

$$\frac{\Omega_0^{\rm gw}(f_1)}{\Omega_0^{\rm gw}(f_2)} = \frac{C_2(k_1)C_3(k_1)}{C_2(k_2)C_3(k_2)}\left[\frac{f_1}{f_2}\right]^{\hat{\alpha}(f_1,f_2)+\hat{n}_t(f_1,f_2)}. \tag{15}$$

Here, $\hat{n}_t(f_1, f_2)$ is given by

$$\hat{n}_t(f_1, f_2) = \frac{1}{\ln(k_1/k_2)} \int_{k_2}^{k_1} n_t(k) \frac{dk}{k}, \tag{16}$$

where $k_{1,2} = 2\pi a_0 f_{1,2}$. And $\hat{\alpha}(f_1, f_2)$ is given by

$$\hat{\alpha}(f_1, f_2) \equiv 2\frac{3\hat{w}(f_1, f_2) - 1}{3\hat{w}(f_1, f_2) + 1}, \tag{17}$$

with

$$\hat{w}(f_1, f_2) \equiv \frac{1}{\ln(a_1/a_2)} \int_{a_2}^{a_1} \tilde{w}(a) \frac{da}{a}, \tag{18}$$

where a_1 and a_2 are, respectively, the values of the scale factor when k_1 and k_2 re-entered the Hubble horizon.

Thus, whereas Eq. (1) shows how long-wavelength (CMB) gravitational-wave constraints relate to shorter-wavelength (pulsar, laser-interferometer, and nucleosynthesis) constraints; Eq. (15) explains how two shorter-wavelength constraints (e.g., from LIGO and LISA) relate to one another.

The second result is obtained by differentiating Eq. (1), which yields a new expression for the logarithmic tilt of the present-day energy spectrum

$$\frac{d\ln\Omega_0^{\rm gw}(f)}{d\ln f} = n_t(k) + 2\left(\frac{3\tilde{w}(k) - 1}{3\tilde{w}(k) + 1}\right) + \frac{d\ln C_2(k)}{d\ln k} + \frac{d\ln C_3(k)}{d\ln k}, \tag{19}$$

where $\tilde{w}(k)$ is the value of the *effective* equation-of-state parameter [see Eq. (8)] when the comoving wave number $k = 2\pi a_0 f$ re-enters the Hubble horizon ($k = aH$).

Note that Eq. (19) generalizes earlier expressions [50,52,53] for $d\ln\Omega_0^{\rm gw}(f)/d\ln f$, by including the corrections arising from the following 3 physical effects, if they are present at the moment when the comoving wave number k is re-entering the Hubble horizon ($k = aH$) in the early universe: (i) first, the term involving $\tilde{w}(k)$ incorporates the correction due to non-negligible bulk viscosity ζ [see Eq. (8)]; (ii) second, the term involving $C_2(k)$ is the correction arising from time variation of the effective equation-of-state parameter $\tilde{w}$; and (iii) the term involving $C_3(k)$ is the correction due to non-negligible tensor anisotropic stress π_{ij}. Again, see Appendix A and Ref. [67] for more details on the correction factors $C_2(k)$ and $C_3(k)$.[4]

Furthermore, if the primordial gravitational-wave spectrum is produced by the amplification of vacuum fluctuations as the mode k "exits the Hubble horizon" in the early universe (as in inflationary, cyclic/ekpyrotic, and pre-big-bang cosmological models), and the equation-of-state parameter is varying sufficiently slowly as k exits the horizon, then $n_t(k)$ is given by

$$n_t(k) = 3 - 3\left|\frac{1 - w_{\rm exit}(k)}{1 + 3w_{\rm exit}(k)}\right| \tag{20}$$

(see Eq. (38) in Ref. [69]), where $w_{\rm exit}(k)$ is the equation-of-state parameter, evaluated at the moment when k exits the Hubble horizon. Note that Eq. (20) applies equally well (i) to expanding models (like inflation, where the modes exit the Hubble horizon while the Universe is expanding with $w < -1/3$); and (ii) to contracting models (like the pre-big bang or cyclic/ekpyrotic models, where the modes exit the horizon while the Universe is contracting with $w > -1/3$).

[4]This generalized expression for $d\ln\Omega_0^{\rm gw}(f)/d\ln f$ is built upon the generalized expression derived in [67] for the gravitational-wave transfer function $T_h(k)$. Then, in Appendix A 2 of the present paper, we obtain a neater and slightly more general expression for $T_h(k)$ by making use of the quantity $\hat{w}(f)$.

V. CMB + LI/PT CONSTRAINTS

In this section, we explore some of the implications of Eq. (1), focusing on the relationship between CMB polarization experiments at long wavelengths and LI and PT experiments at shorter wavelengths. The discussion naturally breaks into $2 \times 2 = 4$ cases, depending on: (i) whether or not CMB polarization experiments have successfully detected r, and (ii) whether or not LI or PT experiments have successfully detected $\Omega_0^{\rm gw}(f)$. We number these cases as shown in Table I, and consider each case in turn.

A. Case 1: neither r nor $\Omega_0^{\rm gw}(f)$ is detected

First suppose that CMB experiments have not yet detected r; and that LI/PT experiments have not yet detected $\Omega_0^{\rm gw}(f)$. Of course, this is the current situation in 2008.

CMB observations provide an upper bound $r \leq r_{\rm max}$. Currently, $r_{\rm max} \approx 0.5$ [65]. It is often claimed that this long-wavelength bound implies an upper bound on $\Omega_0^{\rm gw}(f)$ at shorter wavelengths. Let us examine this claim.

In fact, from Eq. (1), we see that the upper bound is

$$\Omega_0^{\rm gw}(f) \leq [A_1 A_2^{\hat{\alpha}_{\rm max}} A_3^{\hat{n}_{t,\rm max}}] r_{\rm max}, \tag{21}$$

where

$$\hat{\alpha}_{\rm max} = 2\left(\frac{3\hat{w}_{\rm max} - 1}{3\hat{w}_{\rm max} + 1}\right). \tag{22}$$

In other words, in order to infer an upper bound on $\Omega_0^{\rm gw}(f)$ from the CMB upper bound $r \leq r_{\rm max}$, we need to *assume* two additional bounds: $\hat{w}(f) \leq \hat{w}_{\rm max}$ and $\hat{n}_t(f) \leq \hat{n}_{t,\rm max}$. But these two additional bounds are theoretical speculations about the early universe—*not observational facts*—so they should make us nervous. Furthermore, since A_2 and A_3 are huge dimensionless numbers, we see that the upper bound on $\Omega_0^{\rm gw}(f)$ is very sensitive to the assumed values for $\hat{w}_{\rm max}$ and $\hat{n}_{t,\rm max}$.

TABLE I. The analysis in Sec. V breaks into four cases, depending on: (i) whether or not CMB experiments have already detected a nonzero value for r; and (ii) whether or not LI or PT experiments have already detected a nonzero value for $\Omega_0^{\rm gw}(f)$.

	LI/PT nondetection	LI/PT detection
CMB nondetection	Case 1	Case 3
CMB detection	Case 4	Case 2

Now, let us consider the most reasonable *assumptions* about $\hat{w}_{\rm max}$ and $\hat{n}_{t,\rm max}$, given our current theoretical understanding of the early universe.

What is the most reasonable assumption for $\hat{w}_{\rm max}$? First note that, if we assume the bulk viscosity $\zeta(a)$ is nonnegative (as required by the second law of thermodynamics), and we assume that the equation-of-state $w(a)$ satisfies the upper bound $w(a) \leq w_{\rm max}$, then Eqs. (7) and (8) imply that $\hat{w}(f)$ satisfies the *same* upper bound: $\hat{w}_{\rm max} = w_{\rm max}$. Next, note that a fluid of massless (or extremely relativistic) noninteracting particles satisfies $w = 1/3$; and if we give some of these particles finite masses, or finite interactions, this tends to *decrease* w below $1/3$ (see Refs. [67,70]). And in standard reheating/preheating after inflation, one also typically finds $w \leq 1/3$ [71]. For these reasons, and others,

$$\hat{w}_{\rm max} = 1/3 \tag{23}$$

is probably the best guess. But, as argued in Sec. I, there are also perfectly reasonable matter components with $w > 1/3$, and there are even reasons to suspect that these components might generically be important at sufficiently early times (see Fig. 1). Given our current understanding of the early universe, $\hat{w}_{\rm max} = 1/3$ is a good guess—but it is only a guess, and should be checked experimentally.

What is the most reasonable assumption for $\hat{n}_{t,\rm max}$? First note that, if we assume that the primordial tensor tilt $n_t(k)$ satisfies the upper bound $n_t(k) \leq n_{t,\rm max}$, then Eq. (9) implies that $\hat{n}_t(f)$ satisfies the same upper bound: $\hat{n}_{t,\rm max} = n_{t,\rm max}$. If we assume that the primordial gravitational-wave spectrum was generated by inflation, then the primordial tensor tilt is given by the well-known formula $n_t(k) = -2\epsilon(k)$, where $\epsilon(k)$ refers to the value of the parameter $\epsilon(k) \equiv (3/2)(1 + w_{\rm exit}(k)) = -d(\ln H)/d(\ln a)|_k$ when the mode k leaves the Hubble horizon ($k = aH$) during inflation. Then, as long as the stress-energy tensor $T_{\mu\nu}$ during inflation satisfies the so-called "weak-energy condition" (which, as its name suggests, is a very mild assumption, corresponding to $w \geq -1$ in a Friedmann-Lemaitre-Robertson-Walker (FLRW) universe), we can infer $n_t(k) \leq 0$. For these reasons and others,

$$\hat{n}_{t,\rm max} = 0 \tag{24}$$

is probably the best guess. Note that this conclusion is rather general within the context of inflation, in the sense that we have not made reference to scalar fields, or any other details of the (currently unknown) matter content driving inflation. Indeed, the conclusion should be valid as long as the following two conditions hold: (i) gravity may be described (at least effectively) by 4-dimensional general relativity during inflation; and (ii) ϵ is $\ll 1$ and slowly varying during inflation. Both of these conditions are indeed satisfied by most viable inflationary models that have been considered (single-field, multifield, ...), although there are also exotic inflationary models in the literature that can achieve $n_t > 0$, either by violating the weak-energy condition [72] or by modifying gravity [73]. Furthermore, although the upper bound $\hat{n}_{t,\rm max} = 0$ applies to inflationary cosmology, it does *not* apply to other cosmological models in which the perturbations are produced during a contracting phase (e.g., "pre-big-bang" cosmological models, which predict $n_t = 3$ [57], or cyclic/ekpyrotic models, which predict $n_t \approx 2$ [58,60]).

It is perhaps worth adding that, instead of considering inflation in general terms, one may wish to focus on single-field inflation. After all, in 2008, the simplest single-field inflation models (e.g., the quadratic inflaton potential $V(\phi) = (1/2)m^2\phi^2$) continue to agree beautifully with the current cosmological data sets [65], and arguably provide the simplest and most compelling available explanation of those data sets. Since single-field models satisfy the well-known "inflationary consistency relation" $n_t(k_{\rm cmb}) = -r/8$, it turns out that we can make the substitution $\hat{n}_{t,\rm max} \rightarrow -r_{\rm max}/8$ in the upper bound (21), and thereby obtain a somewhat stronger upper bound that is still obeyed by nearly all single-field inflationary models.

To stress that the upper bound on $\Omega_0^{\rm gw}(f)$ at high frequencies is very sensitive to the assumed values for $\hat{w}_{\rm max}$ and $\hat{n}_{t,\rm max}$, we plot this upper bound in Fig. 2, for various choices of $\hat{w}_{\rm max}$ and $\hat{n}_{t,\rm max}$.

Figure 2 also shows the bounds and sensitivities from various current and future gravitational-wave constraints. The LIGO experiment is currently operating at its design sensitivity, and has placed an upper bound $\Omega_0^{\rm gw}(f) < 6.5 \times 10^{-5}$ on the stochastic gravitational-wave background at frequencies near $f \sim 10^2$ Hz [74]. The LIGO sensitivity is expected to increase by another factor of 10–100 within the next year or so [74]. Then, within the next 10 years, Advanced LIGO/VIRGO is expected to reach a sensitivity of $\Omega_0^{\rm gw}(f) \approx 10^{-9} - 10^{-8}$ [74]; and subsequent generations of ground-based LI experiments may do even better. LISA (the first-generation space-based LI experiment) is expected to achieve a sensitivity of $\Omega_0^{\rm gw}(f) \approx 10^{-11}$ at frequencies near $f \sim 10^{-3}$ Hz [75]; and BBO (the second-generation space-based LI experiment, which is specifically designed to detect a stochastic gravitational-wave background) may be able to reach a sensitivity of $\Omega_0^{\rm gw}(f) \approx 10^{-17}$ at frequencies near $f \sim 0.3$ Hz [25,76]. Pulsar-timing experiments have currently placed an upper bound $\Omega_0^{\rm gw}(f) < 2 \times 10^{-8}$ at frequencies between 10^{-9} and 10^{-8} Hz [18]. In the coming years, the Parkes Pulsar Timing Array , which is already operating, should reach a sensitivity of $\Omega_0^{\rm gw}(f) \approx 10^{-10}$ or better at these frequencies [18]; and in the future, the proposed Square Kilometer Array (SKA) experiment may improve this sensitivity by another order of magnitude or more [19]. Finally, if short-wavelength primordial gravitational waves had too much energy density, they would spoil the successful predictions of BBN; so we obtain the sBBN constraint [77–82] depicted in Fig. 2, and further discussed in Sec. VII.

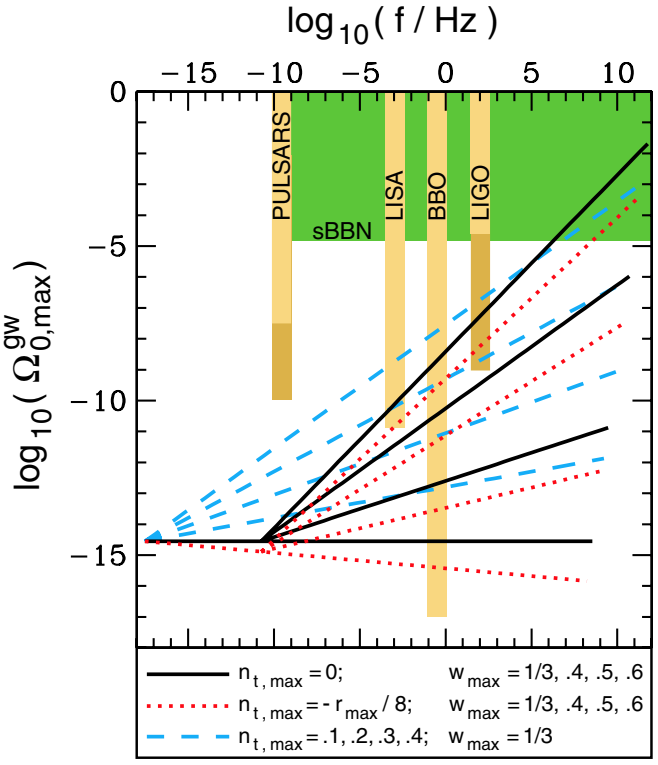

FIG. 2 (color online). This figure relates to "Case 1," discussed in Sec. VA. The curves show the upper bound on $\Omega_0^{\rm gw}(f)$, over the range $f_{\rm cmb} < f < f_{\rm end}$, for various assumed values of $\hat{w}_{\rm max}$ and $\hat{n}_{t,\rm max}$. The four solid black curves correspond (from bottom to top) to $\hat{w}_{\rm max} = \{1/3, 0.4, 0.5, 0.6\}$ and $\hat{n}_{t,\rm max} = 0$. The four dotted red curves show the same thing, but now with $n_{t,\rm max} = -r_{\rm max}/8$. The four dashed blue curves correspond (from bottom to top) to $\hat{n}_{t,\rm max} = \{0.1, 0.2, 0.3, 0.4\}$ and $\hat{w}_{\rm max} = 1/3$. Note that frequencies below $f_c = f_{\rm bbn} \approx 10^{-11}$ Hz reentered the Hubble horizon *after* BBN, and hence are unaffected by assumptions about $\hat{w}$ during the primordial dark age. The current and future experimental constraints shown in the figure are discussed in the text, at the end of Sec. VA.

B. Case 2: both r and $\Omega_0^{\rm gw}(f)$ are detected

If CMB experiments succeed in detecting r, and one of the LI (or PT) experiments (at frequency f) *also* succeeds in detecting $\Omega_0^{\rm gw}(f)$, then Eq. (1) will yield a curve in the $\{\hat{w}(f), \hat{n}_t(f)\}$ plane. This is illustrated in Fig. 3. In fact, this curve will be slightly "fuzzy" due to the nonvanishing error bars on r, $\Omega_0^{\rm gw}(f)$, A_1, A_2, and A_3.

In particular, CMB polarization experiments are expected to be sensitive to a tensor-to-scalar ratio as small as $r = 10^{-2}$, or smaller [13]; and the sensitivities of current and future PT and LI experiments were discussed at the end of Sec. VA. In the top panel of Fig. 3, we imagine that $\Omega_0^{\rm gw}(f)/r = 10^{-7}$ has been detected—e.g., $r = 0.1$ has been detected in the CMB, and $\Omega_0^{\rm gw}(f) = 10^{-8}$ has been detected in one of the LI/PT experiments—and then we plot the corresponding constraint curves, assuming that the detection of $\Omega_0^{\rm gw}(f)$ occurred at a frequency of 10^2 Hz (LIGO), 0.3 Hz (BBO), 10^{-3} Hz (LISA), or 10^{-9} Hz (PT).

And the bottom panel of Fig. 3 illustrates the same thing, assuming that the value of $\Omega_0^{\rm gw}(f)/r$ turns out to be closer to the minimum possible value for each experiment: we use $\Omega_0^{\rm gw}/r = 10^{-9}/0.1 = 10^{-8}$ for LIGO (at 10^2 Hz); and $\Omega_0^{\rm gw}/r = 10^{-17}/0.1 = 10^{-16}$ for BBO (at 0.3 Hz); and $\Omega_0^{\rm gw}/r = 10^{-11}/0.1 = 10^{-10}$ for LISA (at 10^{-3} Hz); and $\Omega_0^{\rm gw}/r = 10^{-11}/0.1 = 10^{-10}$ for SKA (at 10^{-9} Hz). Note that, in Fig. 3, the frequency f is different for each LI/PT experiment: that is, LIGO places a constraint in the $\{\hat{w}(f_{\rm LIGO}), \hat{n}_t(f_{\rm LIGO})\}$ plane, while LISA places a constraint in the $\{\hat{w}(f_{\rm LISA}), \hat{n}_t(f_{\rm LISA})\}$ plane, and so forth.

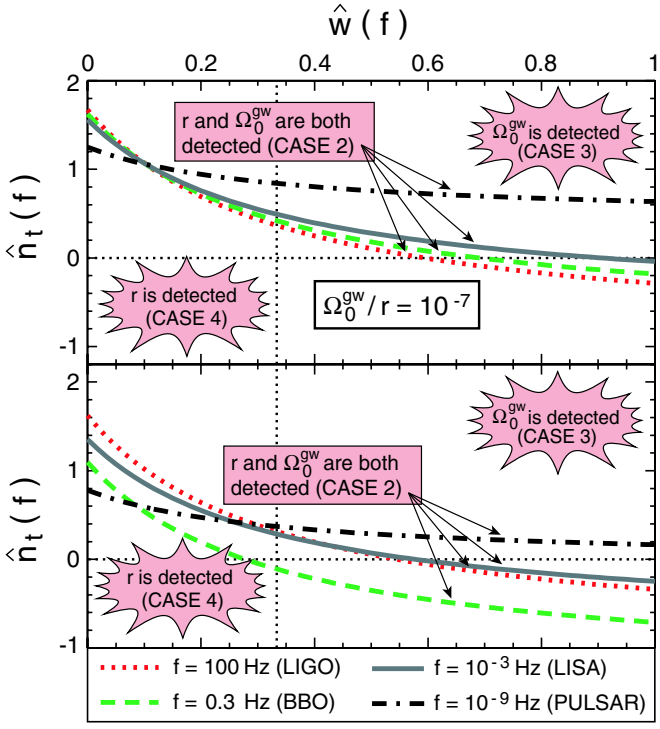

FIG. 3 (color online). Bounds from combining CMB and LI/PT experiments. (This figure relates to Cases 2, 3, and 4, discussed in Secs. VB, VC, and VD.) We show examples of the constraints in the $\{\hat{w}(f), \hat{n}_t(f)\}$ plane that follow from CMB constraints on r and LI/PT constraints on $\Omega_0^{\rm gw}(f)$. In both the top and bottom panels, the four curves correspond to: $f_{\rm LIGO} = 100$ Hz (red dotted); $f_{\rm BBO} = 0.3$ Hz (green dashed); $f_{\rm LISA} = 10^{-3}$ Hz (gray solid); and $f_{\rm pulsar} = 10^{-9}$ Hz (black dotted-dashed). In the top panel, all four curves are plotted assuming $\Omega_0^{\rm gw}(f)/r = 10^{-7}$. So, for example, suppose CMB and LI/PT experiments find: (i) $\Omega_0^{\rm gw}(f) = 10^{-8}$ and $r = 0.1$ (Case 2); or (ii) $\Omega_0^{\rm gw}(f) = 10^{-8}$ and $r < 0.1$ (Case 3); or (iii) $\Omega_0^{\rm gw}(f) < 10^{-8}$ and $r = 0.1$ (Case 4). Then $\{\hat{w}(f), \hat{n}_t(f)\}$ must lie: (i) *on*, (ii) *above*, or (iii) *below* the respective curve. The bottom panel is similar, but instead of all curves corresponding to $\Omega_0^{\rm gw}(f)/r = 10^{-7}$, we take $\Omega_0^{\rm gw}(f)/r$ to be closer to the minimum possible value for each experiment: 10^{-8} (at $f_{\rm LIGO}$); 10^{-10} (at $f_{\rm LISA}$); 10^{-16} (at $f_{\rm BBO}$), and 10^{-10} (at $f_{\rm pulsar}$).

C. Case 3: $\Omega_0^{\rm gw}(f)$ is detected, but r is *not* detected

In this section, let us suppose that one of the LI/PT experiments has successfully detected $\Omega_0^{\rm gw}(f)$ at some frequency f; while CMB experiments have only placed an upper bound on the tensor-to-scalar ratio: $r \leq r_{\rm max}$. We will mention three possible interpretations of this observational situation.

For the first interpretation, we rewrite Eq. (1) as

$$\Omega_0^{\rm gw}(f) \leq [A_1 A_2^{\hat{\alpha}(f)} A_3^{\hat{n}_t(f)}] r_{\rm max}. \tag{25}$$

As in Case 2, this equation defines a curve in the $\{\hat{w}(f), \hat{n}_t(f)\}$ plane. But, whereas in Case 2 the parameters $\hat{w}(f)$ and $\hat{n}_t(f)$ were required to lie *on* this line, in the present situation the parameters are required to lie *above* the line (see Fig. 3).

For the second interpretation, we rewrite Eq. (1) as

$$\hat{w}(f) \geq \hat{w}_{\rm min}(f), \tag{26}$$

where

$$\hat{w}_{\rm min}(f) = \frac{1}{3}\left(\frac{2 + \hat{\alpha}_{\rm min}(f)}{2 - \hat{\alpha}_{\rm min}(f)}\right), \tag{27}$$

and

$$\hat{\alpha}_{\rm min}(f) = -\frac{\ln[A_1 A_3^{\hat{n}_{t,\rm max}(f)} r_{\rm max}/\Omega_0^{\rm gw}(f)]}{\ln[A_2]}. \tag{28}$$

In other words, if we *assume* a theoretical upper bound for $\hat{n}_t(f)$, such as the standard inflationary assumption $\hat{n}_{t,\rm max} = 0$ discussed in Sec. V A, then we can infer that $\hat{w}(f)$ must exceed the lower bound $\hat{w}_{\rm min}(f)$ given by Eqs. (27) and (28). Furthermore, Eqs. (7) and (8) allow us to infer that the effective equation-of-state parameter $\tilde{w}(a)$ must also satisfy the *same* lower bound

$$\tilde{w}(a) \geq \hat{w}_{\rm min}(f) \tag{29}$$

for some nonempty subset of the range $a_k < a < a_c$. And then, if we assume $\zeta(a) \geq 0$ (as required by the second law of thermodynamics), we can also infer that the ordinary equation-of-state parameter $w(a)$ must again satisfy the *same* lower bound

$$w(a) \geq \hat{w}_{\rm min}(f) \tag{30}$$

for some nonempty subset of the range $a_k < a < a_c$.

Equations (27) and (28), for $\hat{w}_{\rm min}(f)$ as a function of $\Omega_0^{\rm gw}(f)/r_{\rm max}$, are plotted in the top panel of Fig. 4, assuming $\hat{n}_{t,\rm max}(f) = 0$ (the standard inflationary assumption, discussed in Sec. V A). The four curves correspond (from top to bottom) to PT experiments at $f \sim 10^{-9}$ Hz (black dotted-dashed curve); LISA at $f \sim 10^{-3}$ Hz (gray solid curve); BBO at $f \sim 0.3$ Hz (green dashed curve); and LIGO at $f \sim 10^2$ Hz (red dotted curve). Since the curves represent $\hat{w}_{\rm min}(f)$, the actual value of $\hat{w}(f)$ must lie *above* these curves.

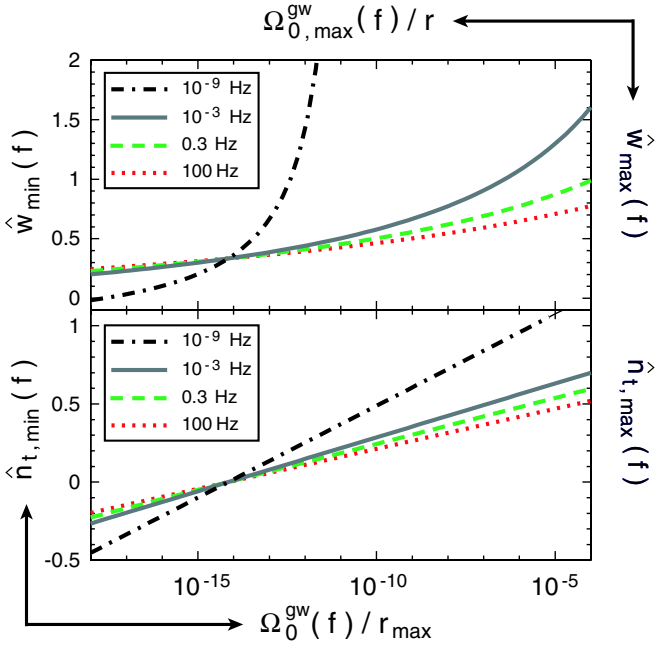

FIG. 4 (color online). Bounds from combining CMB and LI/PT experiments. (This figure relates to Cases 3 and 4, discussed in Secs. V C and V D.) In both the top and bottom panels, the four curves correspond to the four frequencies: $f_{\rm LIGO} = 100$ Hz (red dotted); $f_{\rm BBO} = 0.3$ Hz (green dashed); $f_{\rm LISA} = 10^{-3}$ Hz (gray solid); and $f_{\rm pulsar} = 10^{-9}$ Hz (black dotted-dashed). This figure has two interpretations. In Case 3, where LI (or PT) experiments detect $\Omega_0^{\rm gw}(f)$ and CMB experiments obtain an upper bound $r_{\rm max}$, the "bottom" and "left" axis labels apply, and the curves represent $\hat{w}_{\rm min}(f)$ (top panel, with the standard inflationary assumption $\hat{n}_{t,\rm max} = 0$) and $\hat{n}_{t,\rm min}(f)$ (bottom panel, with the standard primordial-dark-age assumption $\hat{w}_{\rm max} = 1/3$), so the *actual* values of $\hat{w}(f)$ and $\hat{n}_t(f)$ lie *above* the curves. In Case 4, where CMB experiments detect r and LI (or PT) experiments obtain an upper bound $\Omega^{\rm gw}_{0,\rm max}(f)$, the "top" and "right" axis labels apply, and the curves represent $\hat{w}_{\rm max}(f)$ (top panel, with the standard inflationary assumption $\hat{n}_t \approx 0$) and $\hat{n}_{t,\rm max}(f)$ (bottom panel, with the standard primordial-dark-age assumption $\hat{w}(f) \approx 1/3$), so the *actual* values of $\hat{w}(f)$ and $\hat{n}_t(f)$ lie *below* the curves.

For the third interpretation, we rewrite Eq. (1) as

$$\hat{n}_t(f) \geq \hat{n}_{t,\rm min}(f), \tag{31}$$

where

$$\hat{n}_{t,\rm min}(f) = -\frac{\ln[r_{\rm max} A_1 A_2^{\hat{\alpha}_{\rm max}(f)}/\Omega_0^{\rm gw}(f)]}{\ln[A_3]} \tag{32}$$

and

$$\hat{\alpha}_{\rm max}(f) = 2\left(\frac{3\hat{w}_{\rm max}(f) - 1}{3\hat{w}_{\rm max}(f) + 1}\right). \tag{33}$$

In other words, if we *assume* a theoretical upper bound for $\hat{w}(f)$, such as the standard assumption $\hat{w}_{\rm max} = 1/3$ discussed in Sec. V A, then we can infer that $\hat{n}_t(f)$ must

exceed the lower bound $\hat{n}_{t,\min}(f)$ given by Eqs. (32) and (33). Furthermore, from Eq. (9), we can infer that the *actual* primordial tensor power spectrum $n_t(k')$ must also satisfy the *same* lower bound

$$n_t(k') \geq \hat{n}_{t,\min}(f) \tag{34}$$

for some nonempty subset of the range $k_{\rm cmb} < k' < k$.

Equations (32) and (33), for $\hat{n}_{t,\min}(f)$ as a function of $\Omega_0^{\rm gw}(f)/r_{\max}$, are plotted in the bottom panel of Fig. 4, assuming $\hat{w}_{\max}(f) = 1/3$ (a standard assumption about the primordial dark age, as discussed in Sec. V A). Again, the four curves correspond (from top to bottom) to: PT experiments at $f \sim 10^{-9}$ Hz (black dotted-dashed curve); LISA at $f \sim 10^{-3}$ Hz (gray solid curve); BBO at $f \sim 0.3$ Hz (green dashed curve); and LIGO at $f \sim 10^{2}$ Hz (red dotted curve). Since the curves represent $\hat{n}_{t,\min}(f)$, the actual value of $\hat{n}_t(f)$ must lie *above* these curves.

D. Case 4: r is detected, but $\Omega_0^{\rm gw}(f)$ is *not* detected

Finally, in this section, let us suppose that CMB experiments have successfully detected a nonzero value for r, but LI/PT experiments have only managed to place an observational upper bound $\Omega_0^{\rm gw}(f) < \Omega_{0,\max}^{\rm gw}(f)$ at frequency f. As in the previous section, we will mention three possible interpretations of this observational situation.

For the first interpretation, we rewrite Eq. (1) as

$$\Omega_{0,\max}^{\rm gw}(f) \geq [A_1 A_2^{\hat{\alpha}(f)} A_3^{\hat{n}_t(f)}] r. \tag{35}$$

As in Cases 2 and 3, this equation defines a curve in the $\{\hat{w}(f), \hat{n}_t(f)\}$ plane. But, whereas in Case 2 the parameters were required to lie *on* this curve, and in Case 3 the parameters were required to lie *above* this curve, in the present case the parameters are required to lie *below* this curve (see Fig. 3).

For the second interpretation, we rewrite Eq. (1) as

$$\hat{w}(f) \leq \hat{w}_{\max}(f), \tag{36}$$

where

$$\hat{w}_{\max}(f) = \frac{1}{3}\left(\frac{2 + \hat{\alpha}_{\max}(f)}{2 - \hat{\alpha}_{\max}(f)}\right) \tag{37}$$

and

$$\hat{\alpha}_{\max}(f) = -\frac{\ln[r A_1 A_3^{\hat{n}_t(f)}/\Omega_{0,\max}^{\rm gw}(f)]}{\ln[A_2]}. \tag{38}$$

In other words, if we *assume* a standard value for $\hat{n}_t(f)$, then we can infer that $\hat{w}(f)$ must be less than the upper bound $\hat{w}_{\max}(f)$ given by Eqs. (37) and (38). In inflation, the primordial gravitational-wave spectrum is *extremely* flat, so that the "standard" value may be taken as $\hat{n}_t(f) \approx 0$. In fact, the standard inflationary gravitational-wave spectrum has a *slight* negative tilt $n_t(k) = -2\epsilon(k)$, but it is small enough that we can ignore it for the purpose of keeping the present discussion simple. It is enough to note that the slight fuzziness in the standard inflationary value $\hat{n}_t(f) \approx 0$ leads to slight fuzziness in the inferred upper bound $\hat{w}_{\max}(f)$.

Equations (37) and (38), for $\hat{w}_{\max}(f)$ as a function of $\Omega_{0,\max}^{\rm gw}(f)/r$, are plotted in the top panel of Fig. 4, assuming the standard inflationary value $\hat{n}_t(f) \approx 0$. The four different curves correspond to the different LI/PT frequency bands, as already described for Case 3 in Sec. V C. But, in Case 3, these curves represented $\hat{w}_{\min}(f)$, so that the actual value of $\hat{w}(f)$ was required to lie *above* the curves. And now, in Case 4, these same curves represent $\hat{w}_{\max}(f)$, so that the actual value of $\hat{w}(f)$ is required to lie *below* the curves.

For the third interpretation, we rewrite Eq. (1) as

$$\hat{n}_t(f) \leq \hat{n}_{t,\max}(f), \tag{39}$$

where

$$\hat{n}_{t,\max}(f) = -\frac{\ln[r A_1 A_2^{\hat{\alpha}(f)}/\Omega_{0,\max}^{\rm gw}(f)]}{\ln[A_3]} \tag{40}$$

and

$$\hat{\alpha}(f) = 2\left(\frac{3\hat{w}(f) - 1}{3\hat{w}(f) + 1}\right). \tag{41}$$

In other words, if we *assume* a standard value for $\hat{w}(f)$, then we can infer that $\hat{n}_t(f)$ must be less than the upper bound $\hat{n}_{t,\max}(f)$ given by Eqs. (40) and (41). The most common picture of the post-inflationary universe is that, after reheating completes, the Universe settles quickly into ordinary quasi-adiabatic radiation-like expansion [71], so the "standard" value may be taken as $\hat{w}(f) \approx 1/3$. In fact, even during standard quasi-adiabatic radiation-like expansion, various effects—notably conformal anomalies [67,83] and the evolution of g_* and g_{*s} with time [70]—cause w to drop *slightly* below $1/3$, but these corrections are usually small enough that we can ignore them for the purposes of keeping the present discussion simple. It is enough to note that the slight fuzziness in the standard value $\hat{w}(f) \approx 1/3$ leads to a slight fuzziness in the inferred upper bound $\hat{n}_{t,\max}(f)$.

Equations (40) and (41), for $\hat{n}_{t,\max}(f)$ as a function of $\Omega_{0,\max}^{\rm gw}(f)/r$, are plotted in the bottom panel of Fig. 4, assuming a "standard" primordial dark age $\hat{w}(f) \approx 1/3$. The four different curves correspond to the different LI/PT frequency bands, as before. But, in Case 3, these curves represented $\hat{n}_{t,\min}(f)$, so that the actual value of $\hat{n}_t(f)$ was required to lie *above* the curves. And now, in Case 4, these same curves represent $\hat{n}_{t,\max}(f)$, so that the actual value of $\hat{n}_t(f)$ is required to lie *below* the curves.

VI. OBSERVATIONAL CONSISTENCY CHECK

Suppose that a pulsar-timing experiment, or a laser-interferometer experiment like LIGO or LISA, detects a nonzero value for $\Omega_0^{\rm gw}(f)$ that is far above the *expected*

upper bound $\sim 10^{-15}$ which follows from assuming "standard" inflation plus a "standard" primordial dark age (see Sec. V A and Fig. 2). If we wish to interpret this as a detection of the *primordial* gravitational-wave background, then we should expect it to satisfy the following rough consistency check.

If the unexpectedly high value of $\Omega_0^{\rm gw}(f)$ is really due to an unexpectedly high value of $\hat{w}(f)$, or an unexpectedly high value of $\hat{n}_t(f)$, or both, then $\Omega_0^{\rm gw}(f)$ should be very "blue," i.e., rapidly rising with frequency. This point should be intuitively clear from a glance at Fig. 2, but let us be a bit more quantitative. The *standard* expectation is that all four terms on the right-hand-side of Eq. (19) are nearly zero, and hence $\Omega_0^{\rm gw}(f)$ is nearly frequency independent. But if the detected signal is actually due to an unexpectedly high value of $\hat{w}(f)$, then the first term dominates the right-hand-side of Eq. (19), and we expect

$$\frac{d\ln\Omega_0^{\rm gw}}{d\ln f} \gtrsim 2\left(\frac{3\hat{w}_{\rm min}-1}{3\hat{w}_{\rm min}+1}\right), \tag{42}$$

where $\hat{w}_{\rm min}$ is given by Eqs. (27) and (28). And, similarly, if the detected signal is actually due to an unexpectedly high value of $\hat{n}_t(f)$, then the second term dominates the right-hand-side of Eq. (19), and we expect

$$\frac{d\ln\Omega_0^{\rm gw}}{d\ln f} \gtrsim \hat{n}_{t,\rm min}, \tag{43}$$

where $\hat{n}_{t,\rm min}$ is given by Eqs. (32) and (33). These expectations can be checked within the frequency band of a single experiment, or by comparing two different interferometers with two separated frequency bands (like LIGO and LISA).

Note that this is just a consistency check—it does *not* rule out the possibility that the detected gravitational-wave signal is produced by some other source, such as a cosmological phase transition, cosmic strings, or an unanticipated astrophysical source. Furthermore, we have been careful to use the term "expect" rather than "predict" in this section, since it should be clear that Eqs. (42) and (43) are *not* firm predictions. Nevertheless, they are sufficiently strong expectations that—depending on whether or not they are confirmed—they could significantly increase or decrease our confidence in the "Case 2" or "Case 3" interpretations discussed in Secs. V B and V C.

VII. CMB + BBN CONSTRAINTS

In this section, let us suppose that CMB experiments have succeeded in detecting r, and combine this information with the well-known "sBBN constraint [77–82]

$$\int_{f_{\rm bbn}}^{f_{\rm end}} \Omega_0^{\rm gw}(f)\frac{df}{f} \leq 1.5\times 10^{-5}. \tag{44}$$

Note that this constraint only applies to the part of the present-day gravitational-wave spectrum that was generated *prior* to big bang nucleosynthesis; and the integral only runs over frequencies f corresponding to comoving wave numbers k that were already "inside the Hubble horizon" ($k > a_{\rm bbn}H_{\rm bbn}$) at the time of BBN at photon temperature $T \sim 1$ MeV. In particular, the lower integration limit $f_{\rm bbn} \approx 1.8\times 10^{-11}$ Hz corresponds to the mode that was on the Hubble horizon ($k_{\rm bbn} = a_{\rm bbn}H_{\rm bbn}$) at the time of BBN, while the upper integration limit $f_{\rm end}$ corresponds to the high-frequency cutoff of the primordial gravitational-wave spectrum. For example, if the primordial gravitational-wave spectrum was generated by inflation, then the spectrum cuts off exponentially fast for $k > k_{\rm end}$, where $k_{\rm end} = a_{\rm end}H_{\rm end}$ is the comoving wave number that was on the Hubble horizon at the end of inflation. This corresponds to the present-day frequency $f_{\rm end}$ given by Eq. (13).

Although, the sBBN constraint (44) is technically an integral constraint (nonlocal in frequency space), in practice it effectively acts as an algebraic constraint (local in frequency space) of the form $\Omega_0^{\rm gw}(f) < 1.5\times 10^{-5}$ for

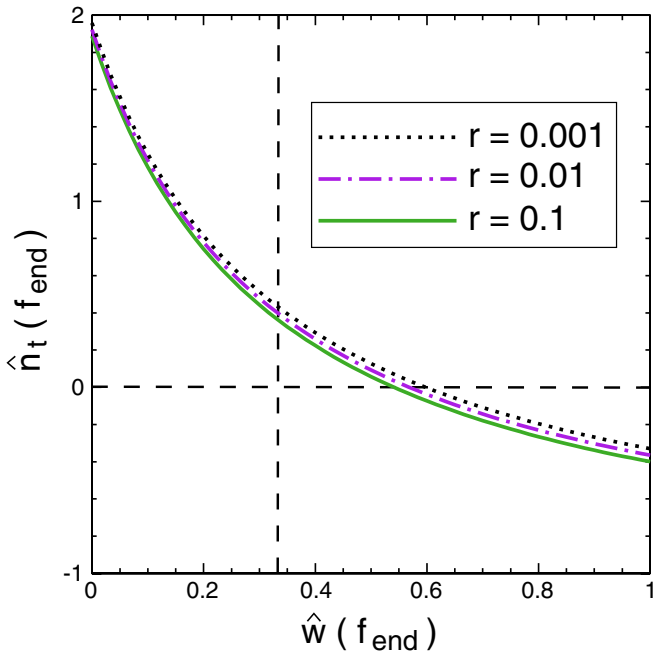

FIG. 5 (color online). Bound from combining sBBN and CMB constraints. If CMB experiments detect r, then the sBBN gravitational-wave constraint immediately requires $\{\hat{w}(f_{\rm end}), \hat{n}_t(f_{\rm end})\}$ to lie *below* the curves shown in the figure. From top to bottom, the curves correspond to: $r = 10^{-3}$ (black dotted curve), $r = 10^{-2}$ (purple dotted-dashed curve), and $r = 10^{-1}$ (green solid curve). Note that the curves are very insensitive to r: they hardly move as r varies over the range in which it can be realistically detected by CMB polarization experiments ($10^{-3} < r < 10^{-1}$). The horizontal and vertical dashed lines point out that, for $r = \{10^{-1}, 10^{-2}, 10^{-3}\}$, respectively: (a) if $\hat{n}_t(f)$ is assumed to take its "standard"' value (≈ 0), then $\hat{w}(f_{\rm end}) \lesssim \{0.54, 0.57, 0.60\}$; and (b) if $\hat{w}(f)$ is assumed to take its "standard" value ($\approx 1/3$), then $\hat{n}_t(f_{\rm end}) \lesssim \{0.36, 0.40, 0.43\}$.

$f_{\rm bbn} < f < f_{\rm end}$. $\Omega_0^{\rm gw}(f)$ can only exceed this bound by having a very narrow spike with $(\delta f)/f_0 \ll 1$, where f_0 is the peak of the spike, and δf is its characteristic width; but (as far as we are aware) there are no known mechanisms for producing such a narrow spike in the primordial gravitational-wave spectrum, and we will neglect this possibility.

Thus, for any frequency f in the range $f_{\rm bbn} < f < f_{\rm end}$, we can directly use all of the equations from "Case 4" in the previous section, as long as we set $\Omega_{0,\rm max}^{\rm gw}(f) = 1.5 \times 10^{-5}$ in those equations. Furthermore, to maximize the length of the "lever arm" between the CMB and BBN constraints, let us consider the case $k \to k_{\rm end}$ and $f \to f_{\rm end}$. Then Eqs. (40) and (41) define a curve in the $\{\hat{w}(f_{\rm end}), \hat{n}_t(f_{\rm end})\}$ plane (shown in Fig. 5), and the actual values of $\hat{w}(f_{\rm end})$ and $\hat{n}_t(f_{\rm end})$ must lie *below* this curve.

Note, in particular, that the constraint curve hardly varies as r varies over the range of realistic future detectability $10^{-3} < r < 10^{-1}$. Furthermore, for $r = \{10^{-1}, 10^{-2}, 10^{-3}\}$, respectively: (a) if $\hat{n}_t(f)$ is assumed to take its "standard" inflationary value ($\hat{n}_t(f) \approx 0$, see Secs. V A and V C), then we obtain the upper bound $\hat{w}(f_{\rm end}) \lesssim \{0.54, 0.57, 0.60\}$; and (b) if $\hat{w}(f)$ is assumed to take its "standard" post-inflationary value ($\hat{w}(f) \approx 1/3$, again see Secs. V A and V C), then we obtain the upper bound $\hat{n}_t(f_{\rm end}) \lesssim \{0.36, 0.40, 0.43\}$.

These results (particularly Fig. 5) are new, and model-independent, constraints on the early universe that will take effect as soon as CMB polarization experiments detect a nonzero value for r.[5]

VIII. CONCLUSION

As far as the early universe is concerned, most people think about upcoming CMB "B-mode" polarization experiments with the following goal in mind: to measure one crucial number, r, which physically corresponds to measuring the energy density of the Universe, roughly 60 e-folds before the end of inflation. But these B-mode experiments will actually achieve significantly more than this: they should also be viewed as half of a two-pronged experiment to detect or constrain the early-universe parameters $\hat{w}(f)$ and $\hat{n}_t(f)$, as we have described in detail. (The other "prong" of this two-pronged experiment is a higher-frequency gravitational-wave constraint coming from laser-interferometer experiments, pulsar-timing measurements, or standard BBN.) For example, if and when CMB experiments detect a nonzero value for r, they will immediately obtain a *supplementary* (and remarkably strong) constraint in the $\{\hat{w}(f_{\rm end}), \hat{n}_t(f_{\rm end})\}$ plane, as shown in Fig. 5. Since quantitative and model-independent constraints on the early universe are notoriously hard to obtain, and we only have a handful, the possibility of obtaining this "supplementary" constraint is exciting.

We have argued that combining large-wavelength constraints on r (from CMB experiments) with small-wavelength bounds on $\Omega_0^{\rm gw}(f)$ (from LI and PT experiments, and sBBN constraints) provides the strongest way to constrain (or detect) the existence and properties of a possible exotic "stiff energy" component (with $w > 1/3$) [37–51] that could have dominated the Universe for some period during the primordial dark age between the end of inflation and the BBN epoch (see Fig. 1).

We have derived several useful and general formulae for relating primordial gravitational-wave constraints at different frequencies, and have shown how these relationships connect to the uncertain physics of the early universe. In Figs. 2–5, we have shown the constraints that will be placed on the parameters $\hat{w}(f)$ and $\hat{n}_t(f)$ by combining various pairs of gravitational-wave constraints, depending on the observational situation (that is, depending on whether CMB and/or LI/PT experiments detect the primordial gravitational-wave background, or only place upper limits).

ACKNOWLEDGMENTS

L. B. thanks Paul Steinhardt for many insightful conversations. A. B. acknowledges support from NSF Grant No. PHY-0603762 and from the Alfred P. Sloan Foundation.

APPENDIX A: DERIVING EQ. (1)

The goal of this appendix is to derive Eq. (A33), which is equivalent to Eq. (1), the basic equation upon which most of the analysis in this paper relies. As a useful and closely related intermediate result, we also obtain Eq. (A32)—an expression for the tensor transfer function $T_h(k)$, which is neater and slightly more general than the tensor transfer function derived in Ref. [67].

The derivation is broken into four parts. In the first part, we review some background material about cosmological gravitational waves, leading to the presentation of Eq. (A7). The second and third parts are devoted to rewriting the factors $T_h(k)$ and $\Delta_h^2(k, \tau_i)$, which appear in Eq. (A7). Finally, in the fourth part, we collect and summarize our results in Eqs. (A32) and (A33).

1. Background material

Let us start by introducing some notation, and reviewing some basic facts about cosmological gravitational waves

[5]Recently, [84] pointed out an interesting new constraint on the cosmic gravitational-wave background, from the fact that gravitational waves act like another decoupled relativistic degree of freedom (i.e., an extra "fraction" of a neutrino species) when the primary CMB fluctuations are generated. For the purposes of this paper, this new CMB constraint is similar to the sBBN constraint analyzed in this section. In the future, the CMB constraint may yield an upper bound on $\Omega_0^{\rm gw}(f)$, which is an order of magnitude tighter than the current sBBN constraint [84]. This improved constraint will slightly lower the curves in Fig. 5.

(tensor perturbations [85]). For more details, see Sec. 2 in Ref. [67].

Tensor metric perturbations in a spatially flat FLRW universe are described by the line element

$$ds^2 = a^2(\tau)[-d\tau^2 + (\delta_{ij} + h_{ij}(\mathbf{x}, \tau))d\mathbf{x}^i d\mathbf{x}^j], \quad \text{(A1)}$$

where $\mathbf{x}$ is a comoving spatial coordinate, τ is a conformal time coordinate, $a(\tau)$ is the FLRW scale factor, and the metric perturbation $h_{ij}(\mathbf{x}, \tau)$ is transverse ($h_{ij,j} = 0$) and traceless ($h_{ii} = 0$). In this appendix we follow the convention that repeated indices (i or j) are summed from 1 to 3.

The tensor power spectrum $\Delta_h^2(k, \tau)$, which represents the contribution by modes of comoving wave number k to the expectation value $\langle h_{ij}(\mathbf{x}, \tau)h_{ij}(\mathbf{x}, \tau)\rangle$, is defined through the equation

$$\langle h_{ij}(\mathbf{x}, \tau)h_{ij}(\mathbf{x}, \tau)\rangle = \int \Delta_h^2(k, \tau)\frac{dk}{k}. \quad \text{(A2)}$$

Note that the expectation value of the left-hand-side is actually independent of $\mathbf{x}$, since a perturbed FLRW universe is *statistically* homogeneous.

CMB and LI experiments measure $\Delta_h^2(k, \tau)$ at very different comoving wave numbers k and very different conformal times τ. In particular, whereas LI experiments measure the *present-day* tensor power spectrum $\Delta_h^2(k, \tau_0)$, CMB experiments may be thought of as measuring the *primordial* tensor power spectrum $\Delta_h^2(k, \tau_i)$. (Here, τ_0 denotes the present time, and τ_i denotes a very early time, before any modes k of interest have had a chance to re-enter the Hubble horizon.) And whereas LI experiments are sensitive to *high* comoving wave numbers (corresponding to length scales smaller than the Solar System), CMB experiments are sensitive to *low* comoving wave numbers (corresponding to large length scales, comparable to the present-day Hubble radius). CMB constraints on the primordial scalar and tensor power spectra, $\Delta_{\mathcal{R}}^2(k, \tau_i)$ and $\Delta_h^2(k, \tau_i)$, are usually quoted at a fiducial "pivot" wave number $k_{\rm cmb}$ in the CMB waveband. For example, the WMAP experiment uses $k_{\rm cmb}/a_0 = 0.002\ {\rm Mpc}^{-1}$, where a_0 is the present-day ($\tau = \tau_0$) value of the FLRW scale factor.

Although it is often convenient, from a theoretical perspective, to work with the tensor power spectrum $\Delta_h^2(k, \tau)$, LI experiments usually report their results in terms of the present-day ($\tau = \tau_0$) gravitational-wave energy spectrum

$$\Omega_0^{\rm gw}(f) \equiv \frac{1}{\rho_0^{\rm crit}}\frac{d\rho_0^{\rm gw}}{d\ln f}, \quad \text{(A3)}$$

where

$$f = \frac{1}{2\pi}\frac{k}{a_0} \quad \text{(A4)}$$

is the present-day physical frequency of a gravitational wave corresponding to the comoving wave number k. Note that the present-day energy spectrum $\Omega_0^{\rm gw}(f)$ is related to the present-day power spectrum $\Delta_h^2(k, \tau_0)$ through the equation

$$\Omega_0^{\rm gw}(f) = \frac{1}{12}\left[\frac{2\pi f}{H_0}\right]^2 \Delta_h^2(k, \tau_0) \quad \text{(A5)}$$

(see Sec. 2 in Ref. [67] for a detailed derivation).

The present-day tensor power spectrum $\Delta_h^2(k, \tau_0)$ is related to the primordial tensor power spectrum $\Delta_h^2(k, \tau_i)$ via the relation

$$\Delta_h^2(k, \tau_0) = T_h(k)\Delta_h^2(k, \tau_i), \quad \text{(A6)}$$

where this equation defines the "tensor transfer function" $T_h(k)$. Combining Eqs. (A5) and (A6) we obtain

$$\Omega_0^{\rm gw}(f) = \frac{1}{12}\left[\frac{2\pi f}{H_0}\right]^2 T_h(k)\Delta_h^2(k, \tau_i). \quad \text{(A7)}$$

This is the basic equation describing the present-day gravitational-wave energy spectrum $\Omega_0^{\rm gw}(f)$ on LI scales. The rest of this section is devoted to rewriting this equation in a more concrete and useful form. In the next two sections, we re-express the two factors $T_h(k)$ and $\Delta_h^2(k, \tau_i)$, respectively.

2. Rewriting the factor $T_h(k)$

First, let us focus on rewriting the factor $T_h(k)$. In this paper, we make use of the general expression for the tensor transfer function $T_h(k)$ derived in Ref. [67]. As explained in Ref. [67], the tensor transfer function $T_h(k)$ may be factored into the form

$$T_h(k) = \tfrac{1}{2}C_1(k)C_2(k)C_3(k). \quad \text{(A8)}$$

The overall factor of $1/2$ comes from averaging over the oscillatory factor $\cos^2(k\tau + \phi(k))$, which appears in the tensor transfer function but is unresolvable in any forseeable LI experiment [86]. Each of the remaining three factors $\{C_1(k), C_2(k), C_3(k)\}$ has a simple physical meaning and is derived in detail in Ref. [67]. Here, we just quote a few key results.

As we shall see, the expression (A8) for $T_h(k)$ is dominated by the factor $C_1(k) \ll 1$, while the other two factors, $C_2(k)$ and $C_3(k)$, represent modest $\mathcal{O}(1)$ corrections.

The factor $C_1(k)$ is given by

$$C_1(k) = \frac{1}{(1 + z_k)^2}, \quad \text{(A9)}$$

where z_k is the redshift at which the mode k re-enters the Hubble horizon ($k = aH$) after inflation. We shall return to this factor below.

The factor $C_2(k)$ is given by

$$C_2(k) = \frac{\Gamma^2(\alpha_k + 1/2)}{\pi}\left[\frac{2}{\alpha_k}\right]^{2\alpha_k}, \quad \text{(A10)}$$

where $\Gamma(x)$ is the gamma function, and we have defined

$$\alpha_k \equiv \frac{2}{1+3\tilde{w}_k}. \tag{A11}$$

Here, $\tilde{w}_k$ is the *effective* equation-of-state parameter at redshift z_k, and is given by

$$\tilde{w}_k = w_k - \frac{8\pi G_N \zeta_k}{H_k}, \tag{A12}$$

where $w_k \equiv p_k/\rho_k$ is the *usual* equation-of-state parameter (i.e., the ratio of the total cosmological pressure p_k to the total cosmological energy density ρ_k), H_k is the Hubble expansion rate, ζ_k is the bulk viscosity of the cosmological fluid (see Secs. 2.11 and 15.11 in Ref. [68])—and, as their subscripts indicate, all of these quantities are evaluated at redshift z_k. C_2 is plotted in Fig. 6. Note that the expression (A10) for $C_2(k)$ is valid as long as the effective equation-of-state parameter $\tilde{w}$ is not changing rapidly relative to the instantaneous Hubble time at redshift z_k; see Ref. [67] for the meaning of $C_2(k)$ more generally.

The factor $C_3(k)$ captures the modification of the primordial gravitational-wave signal due to tensor anisotropic stress π_{ij} (e.g., from free-streaming relativistic particles) in the early universe. In particular, in the important case that the effective equation-of-state near z_k is radiation-like ($\tilde{w} \approx 1/3$), free-streaming relativistic particles with energy density $\rho^{\rm fs}$ damp the gravitational-wave spectrum by the factor

$$C_3(k) = A^2(k), \tag{A13}$$

where

$$A(k) \equiv -\frac{10}{7}\frac{(98\Omega_{\rm fs}^3 - 589\Omega_{\rm fs}^2 + 9380\Omega_{\rm fs} - 55125)}{(15+4\Omega_{\rm fs})(50+4\Omega_{\rm fs})(105+4\Omega_{\rm fs})}, \tag{A14}$$

and $\Omega_{\rm fs} \equiv \rho_k^{\rm fs}/\rho_k^{\rm crit}$ is the fraction of the critical density that is relativistically free-streaming at redshift z_k. C_3 is plotted in Fig. 7.

In the remainder of this section, we focus on obtaining a more explicit expression for $(1+z_k)$ and hence for $C_1(k)$. To do this, let us proceed carefully as follows:

$$\frac{k^2}{a_0^2 H_0^2} = \frac{a_k^2 H_k^2}{a_0^2 H_0^2}, \tag{A15a}$$

$$= \frac{1}{(1+z_k)^2}\frac{\rho_k^{\rm crit}}{\rho_0^{\rm crit}}, \tag{A15b}$$

$$= \frac{\Omega_0^{\rm rad}}{(1+z_k)^2}\frac{\rho_c^{\rm rad}}{\rho_0^{\rm rad}}\frac{\rho_k^{\rm crit}}{\rho_c^{\rm crit}}, \tag{A15c}$$

where $\rho^{\rm rad}$ and $\rho^{\rm crit}$ denote the radiation density and critical density, respectively, and $\Omega_0^{\rm rad} \equiv \rho_0^{\rm rad}/\rho_0^{\rm crit}$. In the first line (A15a), we have used the fact that $k = a_k H_k$ by definition. In the second line (A15b), we have used the definition of the redshift z to write $a_0/a_k = (1+z_k)$, and the definition of the critical density $\rho^{\rm crit}$ to write $H_k^2/H_0^2 = \rho_k^{\rm crit}/\rho_0^{\rm crit}$. In the third line (A15c), we have used the fact that the Universe is radiation dominated at τ_c so that $\rho_c^{\rm crit} = \rho_c^{\rm rad}$.

We have introduced the time τ_c to parametrize our threshold of ignorance: it represents the earliest time at which we *know* that the Universe was already radiation

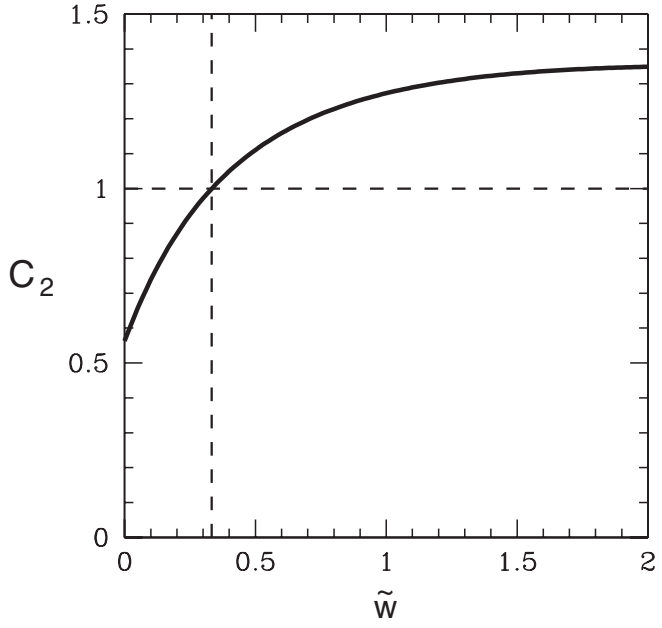

FIG. 6. The correction factor C_2 as a function of the effective equation-of-state parameter $\tilde{w}$, as given by Eqs. (A10) and (A11). Note that $C_2 = 1$ when $\tilde{w} = 1/3$.

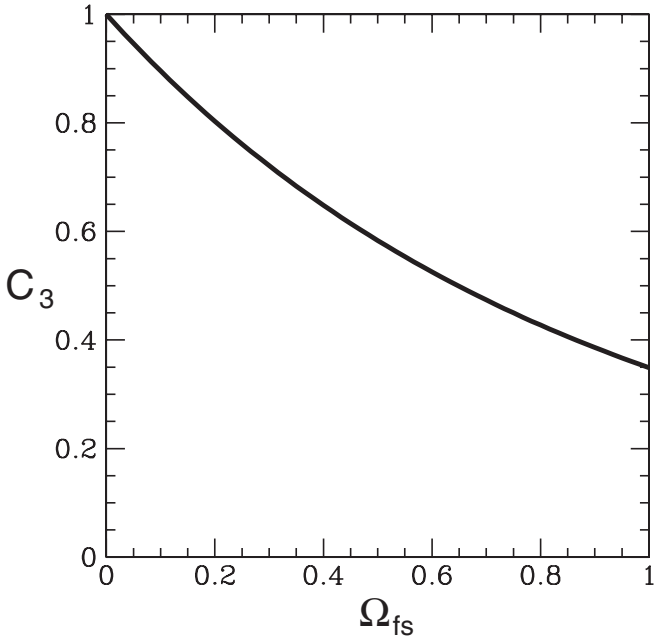

FIG. 7. The correction factor C_3 as a function of the free-streaming fraction $\Omega_{\rm fs} = \rho_k^{\rm fs}/\rho_k^{\rm crit}$, as given by Eqs. (A13) and (A14).

dominated. But, for all we know, the Universe *prior* to τ_c may *not* have been radiation dominated: e.g., an exotic "stiff" component with $w > 1/3$ [38–40] may have dominated the cosmic energy budget. The present agreement between the theoretical and observational understanding of BBN strongly suggests that the Universe was already radiation dominated during BBN (i.e., at the time $\tau_{\rm bbn}$ when the temperature was $T = 1$ MeV), so it currently makes sense to choose $\tau_c = \tau_{\rm bbn}$. But, for the sake of generality, we leave τ_c unfixed in this section, since we can easily imagine future developments—such as an improved understanding of primordial baryogenesis—that would make an earlier time $\tau_c \ll \tau_{\rm bbn}$ a more appropriate choice. Note that for the wave numbers of interest in this paper—e.g., those measured by laser-interferometer experiments—the temporal ordering is $\tau_k < \tau_c < \tau_{\rm eq} < \tau_0$.

Two density ratios appear on the right-hand side of Eq. (A15c). Let us rewrite each of these in turn. In order to rewrite the first ratio, $\rho_c^{\rm rad}/\rho_0^{\rm rad}$, let us pause to review a few properties of an expanding bath of radiation. The bath has energy density ρ and entropy density s given by [see Secs. 3.3 and 3.4 in Ref. [70], and especially Eqs. (3.61), (3.72)]

$$\rho(z) = \tfrac{1}{30}\pi^2 g_*(z) T^4(z), \tag{A16a}$$

$$s(z) = \tfrac{2}{45}\pi^2 g_{*s}(z) T^3(z), \tag{A16b}$$

where $T(z)$ is the temperature at redshift z. These equations may be taken as the *definition* of the quantities $g_*(z)$ and $g_{*s}(z)$, which represent the *effective* number of relativistic degrees of freedom in the radiation bath at redshift z, as measured by the energy density $\rho(z)$ or the entropy density $s(z)$, respectively. If the radiation expands quasi-adiabatically—as is usually the case in the early universe—then the entropy $a^3 s$ remains constant (to a very good approximation). When this is true, Eqs. (A16a) and (A16b) imply that the energy density of the radiation bath redshifts as

$$\frac{\rho^{\rm rad}(z_1)}{\rho^{\rm rad}(z_2)} = \frac{g_*(z_1)}{g_*(z_2)} \frac{g_{*s}^{4/3}(z_2)}{g_{*s}^{4/3}(z_1)} \left(\frac{1+z_1}{1+z_2}\right)^4. \tag{A17}$$

In particular, since the standard radiation epoch begins prior to z_c, the radiation expanded quasi-adiabatically during the epoch $z_c \geq z \geq 0$, so we can write

$$\frac{\rho_c^{\rm rad}}{\rho_0^{\rm rad}} = \frac{g_*(z_c)}{g_*(0)} \frac{g_{*s}^{4/3}(0)}{g_{*s}^{4/3}(z_c)} (1+z_c)^4. \tag{A18}$$

Note that if we know the phase-space distribution functions describing each particle species in the radiation bath, then we can compute the quantities $g_*(z)$ and $g_{*s}(z)$ directly—again see Secs. 3.3 and 3.4 in Ref. [70] for more details. For example, if all relevant particle species are in thermal with one another at temperature T, then $g_* = N_b + (7/8)N_f$ and $g_{*s} = N_b + (7/8)N_f$, where N_b and N_f are the total number of relativistic bosonic and fermionic degrees of freedom, respectively.

To rewrite the second density ratio $(\rho_k^{\rm crit}/\rho_c^{\rm crit})$ appearing in Eq. (A15c), note that conservation of stress energy $(T^{\mu\nu}{}_{;\nu} = 0)$ in the early universe (i.e. in a spatially-flat FLRW universe) implies the continuity equation:

$$\frac{d\rho^{\rm crit}}{\rho^{\rm crit}} = -3[1 + \tilde{w}(a)]\frac{da}{a}. \tag{A19}$$

Here $\tilde{w}(a)$ is the *effective* equation-of-state parameter:

$$\tilde{w}(a) \equiv w(a) - \frac{8\pi G_N \zeta(a)}{H(a)}, \tag{A20}$$

where $w(a) = p(a)/\rho(a)$ is the *usual* equation-of-state parameter [i.e., the ratio of the total cosmological pressure $p(a)$ to the total cosmological energy density $\rho(a) = \rho^{\rm crit}(a)$], $H(a)$ is the Hubble expansion rate, and $\zeta(a)$ is the bulk viscosity of the cosmological fluid (see Secs. 2.11 and 15.11 in Ref. [68]).[6] Integrating Eq. (A19) from $a_c \equiv a(\tau_c)$ to $a_k \equiv a(\tau_k)$ yields

$$\frac{\rho_k^{\rm crit}}{\rho_c^{\rm crit}} = \exp\left\{\int_{a_k}^{a_c} 3[1 + \tilde{w}(a)]\frac{da}{a}\right\}. \tag{A21}$$

Alternatively, we can define an *averaged effective* equation-of-state parameter $\hat{w}(f)$ through the equation

$$\frac{\rho_k^{\rm crit}}{\rho_c^{\rm crit}} = \left(\frac{1+z_k}{1+z_c}\right)^{3[1+\hat{w}(f)]}. \tag{A22}$$

Comparing Eqs. (A21) and (A22), we see that $\hat{w}(f)$ is the logarithmic average of the *effective* equation-of-state parameter $\tilde{w}(a)$ over the range $a_k < a < a_c$

$$\hat{w}(f) = \frac{1}{\ln[a_c/a_k]} \int_{a_k}^{a_c} \tilde{w}(a)\frac{da}{a}. \tag{A23}$$

Note that if $\tilde{w}(a)$ is an a-independent constant over this range (which we DO NOT assume in this paper) then it becomes equal to $\hat{w}$.

Finally, we can plug Eqs. (A18) and (A22) into the right-hand-side of Eq. (A15c), solve for $(1 + z_k)$ and thus find

$$C_1(k) = \frac{1}{(1+z_c)^2}\left[\frac{\gamma^{-1/2}}{(1+z_c)}\frac{2\pi f}{H_0}\right]^{-4/(1+3\hat{w}(f))}, \tag{A24}$$

where we have defined

$$\gamma \equiv \frac{g_*(z_c)}{g_*(0)} \frac{g_{*s}^{4/3}(0)}{g_{*s}^{4/3}(z_c)} \Omega_0^{\rm rad}. \tag{A25}$$

For $g_*(0)$, $g_{*s}(0)$, and $\Omega_0^{\rm rad}$, one should use the values that

[6]Note that, although $\tilde{w}(a)$ may be highly time varying, our calculation does implicitly assume that it satisfies a weak adiabaticity condition with respect to the mode k: after k is well inside the Hubble horizon, the instantaneous time scale for the variation of $w(a)$ should not be shorter than the instantaneous oscillation period of the mode k.

these parameters would have *if all three neutrino species were massless*. (For explicit numerical values, see Appendix C.) These are the correct values to use in Eq. (A25) even though, in reality, neutrinos have mass.

3. Rewriting the factor $\Delta_h^2(k, \tau_i)$

Now, let us focus on rewriting the factor $\Delta_h^2(k, \tau_i)$, i.e., the primordial tensor power spectrum on short wavelengths.

Recall that the tensor spectral index $n_t(k)$ is defined as the logarithmic slope of the *primordial* tensor power spectrum $\Delta_h^2(k, \tau_i)$

$$n_t(k) \equiv \frac{d[\ln\Delta_h^2(k, \tau_i)]}{d[\ln k]}. \tag{A26}$$

Integrating this equation, we obtain

$$\Delta_h^2(k, \tau_i) = \Delta_h^2(k_{\rm cmb}, \tau_i) \exp\left[\int_{k_{\rm cmb}}^{k} n_t(k') \frac{dk'}{k'}\right], \tag{A27}$$

where $\Delta_h^2(k_{\rm cmb}, \tau_i)$ is the primordial tensor power spectrum, evaluated at the CMB "pivot" wave number $k_{\rm cmb}$. Alternatively, we can define an *averaged* spectral index $\hat{n}_t(f)$ through the equation

$$\Delta_h^2(k, \tau_i) \equiv \Delta_h^2(k_{\rm cmb}, \tau_i)[k/k_{\rm cmb}]^{\hat{n}_t(f)}. \tag{A28}$$

In other words, the *effective* spectral index $\hat{n}_t(f)$ is nothing but the logarithmic average of the *actual* spectral index $n_t(k)$ over the wave-number range from $k_{\rm cmb}$ to k

$$\hat{n}_t(f) \equiv \frac{1}{\ln[k/k_{\rm cmb}]} \int_{k_{\rm cmb}}^{k} n_t(k') \frac{dk'}{k'}. \tag{A29}$$

Note that if n_t is a k-independent constant over this range (which we DO NOT assume in this paper) then it becomes equal to $\hat{n}_t$.

Finally, it is conventional (and also convenient, for certain purposes) to define the tensor-to-scalar ratio r through the equation

$$r \equiv \frac{\Delta_h^2(k_{\rm cmb}, \tau_i)}{\Delta_{\mathcal{R}}^2(k_{\rm cmb}, \tau_i)}. \tag{A30}$$

Combining Eqs. (A28) and (A30), we can rewrite $\Delta_h^2(k, \tau_i)$, the primordial tensor power spectrum on short wavelengths, in the form

$$\Delta_h^2(k, \tau_i) = r\Delta_{\mathcal{R}}^2(k_{\rm cmb}, \tau_i)[k/k_{\rm cmb}]^{\hat{n}_t(f)}. \tag{A31}$$

4. Recapitulation

Now, let us assemble our results. Plugging Eq. (A24) into the right-hand-side of Eq. (A8), we obtain the tensor transfer function $T_h(k)$ in the useful form

$$T_h(k) = \frac{C_2(k)C_3(k)}{2(1+z_c)^2}\left[\frac{\gamma^{-1/2}}{(1+z_c)}\frac{2\pi f}{H_0}\right]^{-4/(1+3\hat{w}(f))}, \tag{A32}$$

Then, plugging Eqs. (A31) and (A32) into Eq. (A7), we obtain our final result

$$\Omega_0^{\rm gw}(f) = \frac{r\Delta_{\mathcal{R}}^2(k_{\rm cmb}, \tau_i)C_2(k)C_3(k)\gamma}{24}\left(\frac{\gamma^{-1/2}}{(1+z_c)}\frac{2\pi f}{H_0}\right)^{\hat{\alpha}(f)} \times \left(\frac{a_0H_0}{k_{\rm cmb}}\frac{2\pi f}{H_0}\right)^{\hat{n}_t(f)}, \tag{A33}$$

which is equivalent to Eq. (1) in the text.

In Eqs. (A32) and (A33): $C_2(k)$ is given by Eqs. (A10)–(A12); $C_3(k)$ is given by Eqs. (A13) and (A14); $\hat{w}(f)$ is given by Eq. (A23); γ is given by Eq. (A25); $\hat{n}_t(f)$ is given by Eq. (A29); and we have defined

$$\hat{\alpha}(f) \equiv 2\left(\frac{3\hat{w}(f)-1}{3\hat{w}(f)+1}\right). \tag{A34}$$

Note that, if the quantities $C_2(k)$, $C_3(k)$, $\hat{w}(f)$, and $\hat{n}_t(f)$ are only weakly k dependent, then the frequency-dependences of the tensor transfer function $T_h(k)$ and the present-day gravitational-wave energy spectrum $\Omega_0^{\rm gw}(f)$ are given roughly by $T_h(k) \propto (2\pi f/H_0)^{-4/(1+3\hat{w}(f))}$ and $\Omega_0^{\rm gw}(f) \propto (2\pi f/H_0)^{\hat{\alpha}(f)+\hat{n}_t(f)}$, respectively.

APPENDIX B: DERIVING THE FREQUENCIES f_c AND $f_{\rm end}$

In this appendix we derive Eqs. (12) and (13), for f_c and $f_{\rm end}$, respectively. Let us start with Eq. (12) for f_c. We begin by writing

$$(2\pi f_c)^2 = \frac{a_c^2}{a_0^2}\frac{H_c^2}{H_0^2}H_0^2, \tag{B1a}$$

$$= \frac{H_0^2}{(1+z_c)^2}\frac{\rho_c^{\rm crit}}{\rho_0^{\rm crit}}, \tag{B1b}$$

$$= \frac{H_0^2\Omega_0^{\rm rad}}{(1+z_c)^2}\frac{\rho_c^{\rm rad}}{\rho_0^{\rm rad}}. \tag{B1c}$$

If these steps are unclear, see Eqs. (A15a)–(A15c) and the paragraph that follows them. Now, substituting (A18) into Eq. (B1c), and solving for f_c, we obtain Eq. (12) as desired.

Next let us derive Eq. (13) for $f_{\rm end}$. To begin, note that we can write $\Delta_h^2(k_{\rm end}, \tau_i)$ in two different ways. On the one hand, using Eqs. (A28) and (A30), we can write

$$\Delta_h^2(k_{\rm end}, \tau_i) = r\Delta_{\mathcal{R}}^2(k_{\rm cmb}, \tau_i)\left[\frac{2\pi f_{\rm end}}{k_{\rm cmb}/a_0}\right]^{\hat{n}_t(f_{\rm end})}. \tag{B2a}$$

On the other hand, we can use the well-known inflationary formula

$$\Delta_h^2(k_{\rm end}, \tau_i) = 64\pi G_N\left(\frac{H_{\rm end}}{2\pi}\right)^2, \tag{B2b}$$

where our conventions match those of the WMAP experiment (e.g., see Eq. (A13) in Ref. [64]). Comparing Eqs. (B2a) and (B2b), we see that

$$H_{\rm end}^2 = \frac{\pi^2 r \Delta_{\mathcal{R}}^2(k_{\rm cmb}, \tau_i)}{16\pi G_N}\left(\frac{2\pi f_{\rm end}}{k_{\rm cmb}/a_0}\right)^{\hat{n}_t(f_{\rm end})}. \quad \text{(B3)}$$

Next, from the definition of $f_{\rm end}$, we can write

$$(2\pi f_{\rm end})^2 = \frac{a_{\rm end}^2}{a_0^2} H_{\rm end}^2. \quad \text{(B4)}$$

Note that, since the first factor on the right-hand-side of Eq. (B4) is nothing but $C_1(k_{\rm end})$, we can use Eq. (A24) to rewrite it as

$$\frac{a_{\rm end}^2}{a_0^2} = \frac{1}{(1+z_c)^2}\left[\frac{\gamma^{-1/2}}{(1+z_c)}\frac{2\pi f_{\rm end}}{H_0}\right]^{-4/(1+3\hat{w}(f_{\rm end}))}. \quad \text{(B5)}$$

Finally, we can plug Eqs. (B3) and (B5) into the right-hand-side of Eq. (B4), and solve for $f_{\rm end}$ to obtain Eq. (13) as desired.

APPENDIX C: NUMERICAL FORMULAE

This appendix lists a few useful numbers. From the WMAP 5th-year data [87] we have (with 1σ error bars) $\Delta_{\mathcal{R}}^2(k_{\rm cmb}) = (2.457^{+0.092}_{-0.093}) \times 10^{-9}$ at $k_{\rm cmb} = 0.002/\text{Mpc}$. The present day value of the Hubble expansion rate may be written as $H_0 = (3.24)h \times 10^{-18}$ Hz, where the Hubble parameter $h = 0.701 \pm 0.013$ [87] is a fudge factor that absorbs the uncertainty in the measurement of H_0. Thus, we can write $(2\pi f/H_0) = (1.94/h) \times 10^{18}\ (f/\text{Hz})$. If $k_{\rm cmb} = 0.002\ \text{Mpc}^{-1}$, then $(k_{\rm cmb}/a_0H_0) = 6.00/h$; and if $k_{\rm cmb} = 0.05\ \text{Mpc}^{-1}$, then $(k_{\rm cmb}/a_0H_0) = 150.0/h$. During BBN (at temperature $T = 1$ MeV) we have $(1 + z_{\rm bbn}) = 5.9 \times 10^9$, and the standard values $g_*(z_{\rm bbn}) = g_{*s}(z_{\rm bbn}) = 10.75$ [70]. (Note: for BBN we have used the nice round value $T = 1$ MeV. In the future, if more accuracy is needed, a more accurate value may used, but in practice this would have only a very tiny effect on the figures and bounds obtained in this paper.) From Appendix A in [70], we have the standard values assuming three massless neutrinos: $g_*(0) = 3.3626$, $g_{*s}(0) = 3.9091$, and $\Omega_0^{\rm rad} = 4.3069 \times 10^{-5} h^{-2} (T_{\rm cmb}/2.75\ \text{K})^4$, with $T_{\rm cmb} = 2.725$ K. These are the correct values to use in Eqs. (5) and (A25) for γ, even though neutrinos actually have mass.

[1] P. Ade *et al.* (QUaD Collaboration), arXiv:0705.2359; http://www.stanford.edu/~schurch/quad.html.
[2] K. W. Yoon *et al.* (BICEP Collaboration), arXiv:astro-ph/0606278; http://bicep0.caltech.edu/~bicep/bicep_front.htm.
[3] P. T. Timbie *et al.* (MBI Collaboration), New Astron. Rev. **50**, 999 (2006); http://astro.physics.brown.edu/mbi/.
[4] A. Kogut *et al.* (PAPPA Collaboration), New Astron. Rev. **50**, 1009 (2006); http://chile1.physics.upenn.edu/pappapublic.
[5] A. C. Taylor *et al.* (CLOVER Collaboration), New Astron. Rev. **50**, 993 (2006);
[6] G. Polenta *et al.* (BRAIN Collaboration), New Astron. Rev. **51**, 256 (2007).
[7] PolarBeaR Collaboration, http://bolo.berkeley.edu/polarbear/.
[8] QUIET Collaboration, http://quiet.uchicago.edu/.
[9] Planck Collaboration, http://www.rssd.esa.int/Planck/.
[10] T. E. Montroy *et al.* (SPIDER Collaboration), in *Ground-based and Airborne Telescopes*, edited by Larry M. Stepp [Proceedings of the SPIE 6267, 62670R (2006)]; http://www.astro.caltech.edu/~lgg/spider_front.htm.
[11] P. Oxley *et al.* (EBEX Collaboration), Proc. SPIE Int. Soc. Opt. Eng. **5543**, 320 (2004); http://groups.physics.umn.edu/cosmology/ebex/.
[12] CMBPOL Collaboration, http://universe.nasa.gov/program/inflation.html.
[13] J. Bock *et al.*, arXiv:astro-ph/0604101.
[14] A. G. Polnarev, Sov. Astron. **29**, 607 (1985).
[15] M. Kamionkowski, A. Kosowsky, and A. Stebbins, Phys. Rev. Lett. **78**, 2058 (1997); Phys. Rev. D **55**, 7368 (1997).
[16] U. Seljak and M. Zaldarriaga, Phys. Rev. Lett. **78**, 2054 (1997); M. Zaldarriaga and U. Seljak, Phys. Rev. D **55**, 1830 (1997).
[17] V. M. Kaspi, J. H. Taylor, and M. F. Ryba, Astrophys. J. **428**, 713 (1994).
[18] F. A. Jenet *et al.*, Astrophys. J. **653**, 1571 (2006).
[19] M. Kramer, D. C. Backer, J. M. Cordes, T. J. W. Lazio, B. W. Stappers, and S. Johnston, New Astron. Rev. **48**, 993 (2004).
[20] A. Abramovici *et al.* (LIGO Collaboration), Science **256**, 325 (1992); http://www.ligo.org.
[21] B. Caron *et al.* (VIRGO Collaboration), Classical Quantum Gravity **14**, 1461 (1997); http://www.virgo.infn.it.
[22] H. Lück *et al.* (GEO Collaboration), Classical Quantum Gravity **14**, 1471 (1997); http://geo600.aei.mpg.de/.
[23] M. Ando *et al.* (TAMA Collaboration), Phys. Rev. Lett. **86**, 3950 (2001); http://tamago.mtk.nao.ac.jp.
[24] LISA Collaboration, http://www.lisa-science.org.
[25] E. S. Phinney *et al.* (BBO Collaboration), The Big Bang Observer: NASA Mission Concept Study (2004); G. M. Harry, P. Fritschel, D. A. Shaddock, W. Folkner, and E. S. Phinney, Classical Quantum Gravity **23**, 4887 (2006); **23**, 7361(E) (2006).
[26] S. Kawamura *et al.* (DECIGO Collaboration), Classical Quantum Gravity **23**, S125 (2006).
[27] L. P. Grishchuk, Sov. Phys. JETP **40**, 409 (1975); Ann. N.Y. Acad. Sci. **302**, 439 (1977); A. A. Starobinsky, JETP Lett. **30**, 682 (1979).
[28] A. H. Guth, Phys. Rev. D **23**, 347 (1981); A. D. Linde, Phys. Lett. **108B**, 389 (1982); A. Albrecht and P. J. Steinhardt, Phys. Rev. Lett. **48**, 1220 (1982).
[29] L. F. Abbott and D. D. Harari, Nucl. Phys. **B264**, 487

(1986).
[30] B. Allen, Phys. Rev. D **37**, 2078 (1988).
[31] V. Sahni, Phys. Rev. D **42**, 453 (1990).
[32] L. Krauss and M. White, Phys. Rev. Lett. **69**, 869 (1992).
[33] M. S. Turner, Phys. Rev. D **55**, R435 (1997).
[34] L. Hui and W. H. Kinney, Phys. Rev. D **65**, 103507 (2002).
[35] T. Smith, A. Cooray, and M. Kamionkoswki, Phys. Rev. D **73**, 023504 (2006).
[36] L. A. Boyle, P. J. Steinhardt, and N. Turok, Phys. Rev. Lett. **96**, 111301 (2006).
[37] P. J. E. Peebles and A. Vilenkin, Phys. Rev. D **59**, 063505 (1999).
[38] B. Spokoiny, Phys. Lett. B **315**, 40 (1993).
[39] M. Joyce and T. Prokopec, Phys. Rev. D **57**, 6022 (1998).
[40] B. Ratra and P. J. E. Peebles, Phys. Rev. D **37**, 3406 (1988).
[41] M. Giovannini, Phys. Rev. D **60**, 123511 (1999).
[42] M. Giovannini, Classical Quantum Gravity **16**, 2905 (1999).
[43] A. Riazuelo and J. P. Uzan, Phys. Rev. D **62**, 083506 (2000).
[44] V. Sahni, M. Sami, and T. Souradeep, Phys. Rev. D **65**, 023518 (2001).
[45] H. Tashiro, T. Chiba, and M. Sasaki, Classical Quantum Gravity **21**, 1761 (2004).
[46] D. J. H. Chung, L. L. Everett, and K. T. Matchev, Phys. Rev. D **76**, 103530 (2007).
[47] I. P. Neupane, Classical Quantum Gravity **25**, 125 013 (2008).
[48] L. P. Grishchuk and Yu. V. Sidorov, Classical Quantum Gravity **6**, L161 (1989); Phys. Rev. D **42**, 3413 (1990); L. P. Grishchuk and M. Solokhin, Phys. Rev. D **43**, 2566 (1991).
[49] M. Gasperini, arXiv:hep-th/9607146.
[50] M. Giovannini, Phys. Rev. D **58**, 083504 (1998).
[51] M. Giovannini, Phys. Rev. D **59**, 121301 (1999).
[52] T. Creighton, arXiv:gr-qc/9907045.
[53] N. Seto and J. Yokoyama, J. Phys. Soc. Jpn. **72**, 3082 (2003).
[54] M. Kamionkowski and M. S. Turner, Phys. Rev. D **42**, 3310 (1990).
[55] D. Grin, T. L. Smith, and M. Kamionkowski, Phys. Rev. D **77**, 085020 (2008).
[56] M. Gasperini and G. Veneziano, Phys. Rep. **373**, 1 (2003).
[57] R. Brustein, M. Gasperini, M. Giovannini, and G. Veneziano, Phys. Lett. B **361**, 45 (1995); R. Brustein, arXiv:hep-th/9604159; A. Buonanno, M. Maggiore, and C. Ungarelli, Phys. Rev. D **55**, 3330 (1997); R. Brustein, M. Gasperini, and G. Veneziano, Phys. Rev. D **55**, 3882 (1997); M. Gasperini, Phys. Rev. D **56**, 4815 (1997).
[58] J. Khoury, B. A. Ovrut, P. J. Steinhardt, and N. Turok, Phys. Rev. D **64**, 123522 (2001).
[59] P. J. Steinhardt and N. Turok, Science **296**, 1436 (2002); Phys. Rev. D **65**, 126003 (2002).
[60] L. A. Boyle, P. J. Steinhardt, and N. Turok, Phys. Rev. D **69**, 127302 (2004).
[61] A. J. Farmer and E. S. Phinney, Mon. Not. R. Astron. Soc. **346**, 1197 (2003).
[62] S. Y. Khlebnikov and I. I. Tkachev, Phys. Rev. D **56**, 653 (1997); R. Easther and E. A. Lim, J. Cosmol. Astropart. Phys. 04 (2006) 010; R. Easther, J. T. Giblin, and E. A. Lim, Phys. Rev. Lett. **99**, 221301 (2007); J. Garcia-Bellido and D. G. Figueroa, Phys. Rev. Lett. **98**, 061302 (2007); J. Garcia-Bellido, D. G. Figueroa, and A. Sastre, Phys. Rev. D **77**, 043517 (2008); J. F. Dufaux, A. Bergman, G. N. Felder, L. Kofman, and J. P. Uzan, Phys. Rev. D **76**, 123517 (2007).
[63] E. Witten, Phys. Rev. D **30**, 272 (1984); C. Hogan, Mon. Not. R. Astron. Soc. **218**, 629 (1986); A. Kosowsky, M. S. Turner, and R. Watkins, Phys. Rev. D **45**, 4514 (1992); Phys. Rev. Lett. **69**, 2026 (1992); A. Kosowsky and M. S. Turner, Phys. Rev. D **47**, 4372 (1993); M. Kamionkowski, A. Kosowsky, and M. S. Turner, Phys. Rev. D **49**, 2837 (1994); C. Grojean and G. Servant, Phys. Rev. D **75**, 043507 (2007).
[64] H. V. Peiris *et al.* (WMAP Collaboration), Astrophys. J. Suppl. Ser. **148**, 213 (2003).
[65] D. N. Spergel *et al.* (WMAP Collaboration), arXiv:astro-ph/0603449.
[66] A. Lewis, A. Challinor, and A. Lasenby, Astrophys. J. **538**, 473 (2000); http://camb.info/.
[67] L. A. Boyle and P. J. Steinhardt, Phys. Rev. D **77**, 063504 (2008).
[68] S. Weinberg, *Gravitation and Cosmology: Principles and Applications of the General Theory of Relativity* (Wiley, New York, 1972).
[69] L. A. Boyle, P. J. Steinhardt, and N. Turok, Phys. Rev. D **70**, 023504 (2004).
[70] E. W. Kolb and M. S. Turner, Front. Phys. **69**, 1 (1990).
[71] D. I. Podolsky, G. N. Felder, L. Kofman, and M. Peloso, Phys. Rev. D **73**, 023501 (2006).
[72] M. Baldi, F. Finelli, and S. Matarrese, Phys. Rev. D **72**, 083504 (2005).
[73] J. Khoury, Phys. Rev. D **76**, 123513 (2007).
[74] B. Abbott *et al.* (LIGO Scientific Collaboration), arXiv: astro-ph/0608606.
[75] C. Ungarelli and A. Vecchio, Phys. Rev. D **64**, 121501 (2001).
[76] C. Cutler and J. Harms, Phys. Rev. D **73**, 042001 (2006).
[77] V. F. Schwartzmann, JETP Lett. **9**, 184 (1969).
[78] Ya. B. Zeldovich and I. D. Novikov, *Structure and Evolution of the Universe* (Moscow, Nauka, 1975).
[79] B. J. Carr, Astron. Astrophys. **89**, 6 (1980).
[80] B. Allen, arXiv:gr-qc/9604033.
[81] M. Maggiore, Phys. Rep. **331**, 283 (2000).
[82] R. H. Cyburt, B. D. Fields, K. A. Olive, and E. Skillman, Astropart. Phys. **23**, 313 (2005).
[83] H. Davoudiasl, R. Kitano, G. D. Kribs, H. Murayama, and P. J. Steinhardt, Phys. Rev. Lett. **93**, 201301 (2004).
[84] T. L. Smith, E. Pierpaoli, and M. Kamionkowski, Phys. Rev. Lett. **97**, 021301 (2006).
[85] J. M. Bardeen, Phys. Rev. D **22**, 1882 (1980).
[86] B. Allen, E. E. Flanagan, and M. A. Papa, Phys. Rev. D **61**, 024024 (1999).
[87] E. Komatsu *et al.* (WMAP Collaboration), arXiv:0803.0547.